Volatile Organic Compounds and Ozone in Rocky Mountain National Park during FRAPPÉ

Katherine B. Benedict[1], Yong Zhou[1], Barkley C Sive[2], Anthony J. Prenni[2], Kristi A. Gebhart[3], Emily V. Fischer[1], Ashley Evanoski-Cole[1], Amy P. Sullivan[1], Sara Callahan[1], Bret A. Schichtel[3], Huiting Mao[4], Ying Zhou[4], Jeffrey L. Collett, Jr. [1]

[1]Department of Atmospheric Science, Colorado State University, Fort Collins, CO 80523, USA
[2]National Park Service, Air Resources Division, Lakewood, CO 80225, USA
[3]National Park Service, Air Resources Division, Fort Collins, CO 80523, USA
[4]Department of Chemistry, State University of New York College of Environmental Science and Forestry, Syracuse, NY, 13210, USA

Correspondence to: Katherine B. Benedict (katherine.benedict@colostate.edu)

Abstract. The 2014 Front Range Air Pollution and Photochemistry Éxperiment (FRAPPÉ) aimed to better characterize summertime air quality in the Northern Front Range Metropolitan Area (NFRMA) and its impact on surrounding areas. As part of this study, measurements of gas and particle phase species were collected in Rocky Mountain National Park (ROMO), located in the mountains west of the urban North Front Range corridor. We report on measurements of ozone from two locations in the park and a suite of volatile organic compounds (VOCs) measured using a continuous real-time gas chromatography system and a quadrupole proton-transfer reaction-mass spectrometer at the ROMO Longs Peak air quality site. We also measured VOCs using canister samples collected along transects connecting the NFRMA and ROMO. These datasets show that ROMO is impacted by NFRMA emission sources, and high observed mixing ratios of VOCs associated with oil and gas extraction (e.g. ethane) and urban sources (e.g. ethene and C_2Cl_4) occur during periods of upslope transport. Hourly ozone mixing ratios exceeded 70 ppb on six events. Two of the six events were largely associated with VOCs from the oil and gas sector, three high ozone events were associated with a mixture of VOCs from urban and oil and gas sources, and one high ozone event was driven by a stratospheric intrusion. For the high ozone events most associated with emissions from oil and gas activities, we estimate that VOCs from this sector contributed to ~20 ppbv of additional ozone.

1. Introduction

Ozone (O_3) is a regulated pollutant that can impact both human and ecosystem health. Monthly mean daytime O_3 has been increasing in the Rocky Mountains and throughout much of the west (Strode et al., 2015), and there are concerns about O_3 levels and exceedances of the O_3 National Ambient Air Quality Standard (NAAQS) at high elevation sites (Christensen et al., 2015; Musselman and Korfmacher, 2014). In Rocky Mountain National Park (ROMO), a protected Class I area with

millions of visitors each year (National Park Service, 2017), O_3 mixing ratios often exceed the current NAAQS standard of 70

ppb and vegetation injury thresholds (Kohut et al., 2012). A timeline of O_3 mixing ratios measured at the ROMO Longs Peak

(ROMO-LP) CASTNET (Clean Air Status and Trends NETwork) site from January 2010 to December 2015 is shown in Figure

1. In addition to transport and O_3 production from regional source emissions, the U.S. Intermountain West (all elevations) has

5   a higher probability of stratospheric O_3 reaching the troposphere from tropopause folding (related to mid-latitude jet or cutoff

low) and stratospheric intrusion events (Lin et al., 2015; Musselman and Korfmacher, 2014; Reddy and Pfister, 2016;

Wooldridge et al., 1997). At Great Basin National Park, another high elevation park in the west, elevated O_3 mixing ratios

have been shown to be impacted by long-range transport, regional transport, and high-altitude transport (Christensen et al.,

2015), highlighting the complex nature of O_3 sources at these Intermountain West sites.

10   ROMO is in close proximity to the North Front Range Metropolitan Area (NFRMA), which includes Denver,

Boulder, and Fort Collins (urban areas) (Figure 2), in addition to the Denver-Julesburg Basin, which has seen significant

increases in oil and natural gas production. For example, in nearby Weld County, the number of active wells doubled between

January 2008 and July 2015, to over 27,000 [Colorado Oil and Gas Conservation Commission (COGCC) 2/2016]. Previous

studies have extensively characterized NFRMA volatile organic compound (VOC) emissions, including those from oil and

15   natural gas extraction activities, and their influence on air quality at the Boulder Atmospheric Observatory (Gilman et al.,

2013; McDuffie et al., 2016; Pétron et al., 2012; Swarthout et al., 2013). These studies demonstrate the extremely high mixing

ratios of alkanes in the NFRMA, with maximum observed ethane and propane mixing ratios exceeding 100 ppbv (Swarthout

et al., 2013) compared to mean values of 0.56-8.74 ppbv and 0.29-6.05 ppbv, respectively, in urban areas (Baker et al., 2008).

The extent that these emissions reach ROMO has not been previously determined, although previous studies have shown that

20   agricultural ammonia emissions from a similar geographic source region are frequently transported into ROMO (Beem et al.,

2010; Benedict et al., 2013).

         The Front Range Air Pollution and Photochemistry Experiment (FRAPPÉ) took place in the summer of 2014 and was

focused on characterizing summertime air quality and O_3 formation in the NFRMA. FRAPPÉ included extensive ground,

mobile and aircraft measurements throughout the region, including ROMO. This work focuses on a primary goal of the

25   measurements at ROMO – to better understand the factors contributing to high O_3 in the park including potential contributions

of the NFRMA. These data are meant to inform strategies to reduce O_3 in the park and the exposure of visitors and ecosystems to elevated O_3 levels. Measurements at the ROMO Longs Peak site (40.2783°N, 105.5457°W; 2784 m ASL) during FRAPPÉ included a suite of VOCs in addition to O_3 and meteorological parameters, which are routinely measured at the site. Whole air canister samples were also collected along U.S. Route 34 from the NFRMA to higher elevation sites (3600 m) to examine

5   spatial variations in VOC concentrations (Figure 2). Ozone and meteorological measurements were also made at an additional high elevation site within ROMO, located off Trail Ridge Road (ROMO-TR; 40.3900° N, 105.6865° W, 3498 m ASL). Additional measurements carried out at ROMO during FRAPPÉ are the focus of separate publications (Benedict et al., in review; Zaragoza et al., 2017).

2. Methods

10   ### 2.1 In situ Volatile Organic Compound Measurements

A cryogen-free concentration system coupled with two gas chromatographs (GC) was installed in the Colorado State University Mobile Laboratory for near real-time (1-hr sample frequency) analysis of VOCs at the Longs Peak Monitoring Station at ROMO from 17 July to 4 September 2014. Ambient air was drawn from 5.25 m above ground level using a 3 m × 0.635 cm outer diameter (o.d.) stainless steel line followed by a 3 m × 0.4 cm inner diameter (i.d.) PFA line. Air flow was

15   maintained continuously at ~7 L min^{-1} using a metal bellows pump (MB-158, Senior Flexionics, Sharon, MA) and delivered a pressure of 10 psig. The inlet residence time was <1 s. A sub-stream of the pressurized air (~2.5 L min^{-1}) was directed to a water management system, which reduced water vapor before entering the analytical system. The water management system consisted of a 7.5 m × 0.635 cm o.d. stainless steel coil and a stainless steel liquid water reservoir, which was housed in a commercial refrigerator and set at ~2° C. The total volume of the system was ~380 ml, yielding a residence time of <10 s.

20   The VOC analytical system was similar to those used in previous studies (Abeleira et al., 2017; Sive et al., 2005) and utilized a Qdrive 2s102K cryocooler (Chart, Inc., Troy, NY) that was capable of cooling a sample enrichment loop from 100 °C to -180 °C in 25 minutes for sample concentration. Additional details are provided in the supplemental information. Two different whole air standards were alternately analyzed every 10 samples throughout the campaign for quantification of the target gases as well as to monitor the system's performance. The measurement precision, represented by the relative standard deviation

(RSD) of the peak areas for each compound in the standards, was 1-8% for the non-methane hydrocarbons (NMHCs), 3-11%

for halocarbons, and 3-5% for alkyl nitrates. A list of VOCs measured during this study using the *in situ* GC is shown in Table

1.

2.2.1 Canister sampling

5   Whole air canister samples were collected at eight non-urban locations during the campaign to investigate the spatial

distributions of VOCs. Canister samples were collected in the Big Thompson Canyon along Route 34 en route to the ROMO

Longs Peak site three days a week during the campaign; several transects were also continued up Trail Ridge Road to the

continental divide at the Alpine Visitors Center in ROMO (ROMO-TR, Figure 2) when upslope transported was expected. A

total of 39 individual VOCs were quantified from the canister samples in our laboratory at Colorado State University using a

10 five-channel, three-GC analytical system, which employed three FIDs, one ECD and one mass spectrometer (MS). The gases

analyzed included C_2-C_{10} NMHCs, C_1-C_2 halocarbons, C_1-C_5 alkyl nitrates, selected reduced sulfur compounds and OVOCs.

A complete list of VOCs measured from the canister samples using the lab analytical system is included in Table 1.

      The analytical system and methodology used for this study are similar to those used in previous studies (Russo et al.,

2010b; Sive, 1998; Zhou et al., 2010). Multiple standards were used during sample analysis (analyzed every 10 samples). The

15 measurement precision, represented by the relative standard deviation (RSD) of the peak areas for each compound in the whole

air standards, was 1-8% for the NMHCs, 3-10% for halocarbons, and 3-5% for the alkyl nitrates.

2.2.2   Proton Transfer Reaction-Mass Spectrometer (PTR-MS)

      Selected VOCs and OVOCs were monitored in real-time by a quadrupole proton-transfer reaction-mass spectrometer

located in the NPS air quality monitoring shelter (PTR-MS; Ionicon Analytik, Innsbruck, Austria) from 14 July to 8 September

20 2014. The PTR-MS sampled air that was continuously drawn through a 13 m × 1.27 cm o.d. (0.9525 cm i.d.) PFA Teflon inlet

from 10 m above ground level. The flow rate through the sample line was ~70 L min^{-1}, resulting in a <1 s residence time. A

diaphragm pump was used to draw a sub-stream of air off the main inlet line through a 1 m × 0.635 cm PFA Teflon line at a

flow rate of 1 L min^{-1} from which the PTR-MS sampled.

The PTR-MS was operated with a drift tube pressure and temperature of 2.0 mbar and 45 °C, respectively, and a potential of 600 V applied over the length (9.6 cm) of the drift tube. The ion source water flow rate was 11 ml min^{-1} and the discharge current was 8 mA. A series of 30 masses was monitored continuously; six masses were monitored for diagnostic purposes while the remaining 24 masses corresponded to VOCs of interest. The dwell time for each of these 24 masses ranged

5   from 1-10 s, yielding a total measurement cycle of ~3 min. The system was zeroed every 25 hours for 10 cycles by diverting the flow of ambient air through a heated catalytic converter (0.5% Pd on alumina at 550 °C) to determine system background signals. Calibrations for the PTR-MS system were conducted using three different high-pressure cylinders containing synthetic blends of selected NMHCs and OVOCs at ppbv levels. Each of the cylinders used in the calibrations had an absolute accuracy of <±5% for all gases. Standards were diluted to atmospheric mixing ratios (ppbv to pptv levels) with catalytic converter-

10   prepared zero air adjusted to maintain the humidity of the sampled air for 6-10 cycles every 25-75 hours. Mixing ratios for each gas were calculated by using the normalized counts per second which were obtained by subtracting out the non-zero background signal for each compound. The PTR-MS precision was estimated from counting statistics and ranged from 6-15%.

2.3 Ozone measurement at Longs Peak and Trail Ridge Road

2.3.1 Trail Ridge Road

15   The third generation of a custom built portable O$_3$ monitoring system (POMS3, Air Resource Specialists, Inc., Fort Collins, CO) was deployed at a high elevation site located off of the Ute Trail in ROMO (40.3900˚ N, 105.6865˚ W, 3498 m ASL) during FRAPPÉ for O$_3$ and meteorological measurements. Measurements were conducted from 11 July – 18 September 2014. The system incorporated two 2B Technologies O$_3$ analyzers, a 6.1 m sampling mast, a data acquisition system, and meteorological instruments for measurements of wind speed, wind direction, temperature, relative humidity, solar radiation,

20   and precipitation. The POMS3 unit was fitted with solar panels and batteries sufficient for operation during the campaign. Hourly averages of O$_3$ and meteorological parameters were reported for this site. More information on the Trail Ridge O$_3$ measurements and calibration procedures can be found in the supplement.

2.3.2 Longs Peak

Ozone and meteorological measurements have been measured continuously at the ROMO Longs Peak site since 1987, as part of the National Park Service Gaseous Pollutant Monitoring Program. As a regulatory O_3 monitoring station, the sampling methods for gaseous and meteorological monitoring are based on the 40 CFR Part 58 requirements. The Longs Peak

5 site includes a temperature-controlled shelter that houses the O_3 analyzer and calibration system. The O_3 inlet and meteorological measurements are located on top of a 10-m tower. Ozone is measured by UV absorption utilizing a Thermo 49i O_3 analyzer coupled with a Thermo 49i O_3 reference station for nightly zero, precision and span checks. One minute O_3 data are recorded and hourly averages are generated from the 1-minute O_3 data. The suite of meteorological measurements include wind speed, wind direction, relative humidity, temperature, solar radiation and precipitation, and 1-minute

10 meteorological data were acquired during FRAPPÉ. As with the POMS3 site, further details can be found in the Gaseous Pollutant Monitoring Program 2015 Quality Assurance Project Plan (https://ard-request.air-resource.com/Project/documents.aspx).

2.4 Data filtering to remove local source effects

Initial analysis of FRAPPÉ data showed unexpectedly high propane concentrations relative to other VOCs at the

15 ROMO-LP site. The highest propane concentrations were associated with the lowest wind speeds, suggesting that a leaking propane tank used by a nearby camp (<200 m) was a local source. Typically in the U.S., propane fuel is primarily propane (at least 90%), with the composition balance mostly containing ethane, propene, butane, and odorants. This is the HD-5 standard, Heavy Duty-5% maximum allowable propene content, and no more than 5% butanes and ethane defined by the American Society for Testing and Materials by Standard 1835 for internal combustion engines.

20 To better understand the influence of regional VOC emissions and transport on the distributions of VOCs and O_3 in ROMO, it was necessary to filter out alkane, alkene, and BTEX (benzene, toluene, ethylbenzene, xylene) data that were affected by the local emissions. In this study, data with ethane/propane ratios <1 were considered to be propane tank influenced and were removed. The resulting ratio of ethane to propane for filtered data (1.2) was similar to that determined for transect samples (1.13) taken at multiple locations in ROMO at different times, supporting the data-filtering approach.

3.0 Temporal and Spatial Trends

3.1 Volatile Organic Compounds

Throughout the campaign, hourly VOC mixing ratios varied by 1 to 3 orders of magnitude (Table 1). Figure 3 and Figure S1 show this variability for several VOCs as well as for O_3 at the ROMO-LP and ROMO-TR sites from 17 July - 4

5   September, 2014. The C_2-C_5 alkanes, C_2-C_4 alkenes, ethyne, aromatics (benzene and toluene), C_2-C_5 alkyl nitrates, tetrachloroethylene (C_2Cl_4), trichloroethylene (C_2HCl_3) and OVOCs, such as methanol, generally had similar temporal variations during most of the study period. The similar temporal patterns suggest that many of the concentration changes are driven by meteorology, with westerly flow generally transporting cleaner air, and easterly flow transporting pollutants from the NFRMA. However, in some cases, differences between species' mixing ratio enhancements likely reflect specific sources

10   influencing air masses that reach the park.

All of the VOCs from Figure 3 have sources in the NFRMA. For example, light alkanes (e.g. ethane) have oil and natural gas sources in northeastern Colorado and have been observed in high abundance along the Front Range (Abeleira et al., 2017; Gilman et al., 2013; Swarthout et al., 2013). Vehicle combustion, prevalent throughout the NFRMA, is an important source of light alkenes, ethyne, and aromatics (e.g. benzene) (Koppmann, 2007), although oil and gas emissions have also

15   been shown to be the most important source of aromatics, specifically benzene, at certain locations (Abeleira et al., 2017; Halliday et al., 2016). C_2Cl_4 and C_2HCl_3 are widely used as solvents and dry cleaning fluids and are frequently used as tracers of urban air masses (Blake et al., 1996). Methanol has vegetative sources, but, more importantly for the Front Range, this trace gas also comes from animal agriculture and confined animal feeding operations (CAFOs).

To better understand VOC influence from these sources, air mass transport patterns were examined with hourly 2-

20   day ensemble back trajectories started at 10 m above ground using the Hybrid Single-Particle Lagrangian Integrated Trajectory (HYSPLIT) model ver 4.9 (Stein et al., 2015). Input data are from the North American Model with a grid resolution of 12 km (NAM12) (Janjic, 2003). Back trajectory residence time analyses are a long-established method to examine upwind air mass transport pathways for periods of interest (Ashbaugh et al., 1985). Previous back trajectory analyses for ROMO captured most meso-synoptic scale patterns, but may underestimate the easterly upslope flow into the park (Gebhart et al., 2011, 2014). In

25   Figure 4a, the Overall Residence Time (ORT) shows the relative probability for transport from the areas upwind of ROMO-

LP during all hours of the study without regard to observed air mass composition. Results indicate that during the study period, air masses arrived from all directions, but areas most frequently upwind were areas to the southwest and the Front Range. Similarly, High Mixing Ratio Residence Times (HRT) were generated using only hours when a measured VOC mixing ratio at ROMO-LP exceeded the 90th percentile of study values. The HRT for ethane, which primarily is from leakage during the

5 production and transport of natural gas (Tzompa-Sosa et al., 2017), is shown in Figure 4b. A sparser pattern results from including only 10% of the hours. Many of the same areas are upwind as in the ORT, but areas to the east have a higher probability of being upwind during this subset of high concentration time periods.

Figure 5 presents differences between transport patterns during high mixing ratio measurements (exceeding the 90th percentile), as compared to all study conditions. The difference maps in Figure 5 are calculated by subtracting the overall

10 probability of transport (ORT) from the probability of transport on a high mixing ratio hour (HRT), or HRT-ORT (Poirot et al., 2001) . Figure 5a shows the results for ethane (Figure 4b – Figure 4a). This more clearly shows that high concentrations

of ethane are preferentially associated with transport from northeastern Colorado, where large oil and gas emissions occur (Figure 2). Figure 5b shows a similar analysis, but for C_2Cl_4 (urban tracer) measurements. The results again point to the NFRMA, but with more of an influence from further south toward Denver because of its widespread usage in the region.

15 Figure 5c shows results for isoprene. In this case, wooded mountainous areas to the west are upwind more often than average. Plots for ethene (tracer for fuel combustion) (Figure 5d) and ethyne (not shown) also point to the NFRMA. These results are not surprising, as upslope conditions are expected to transport pollutants to the park. However, this is the first time that *in situ* VOC tracers have been used to demonstrate the many Front Range sources that impact ROMO.

NMHC levels observed at ROMO can be of a comparable magnitude to other urban/industrial regions, further

20 suggesting a significant impact of the polluted NFRMA on the park. The observed mixing ratios of light NMHCs from this study are compared to those reported at other locations in Figure 6. With the exception of benzene and ethyne, measured mixing ratios from the transect samples (gray) and other measurements made in the Front Range (Abeleira et al., 2017; McDuffie et al., 2016; Swarthout et al., 2013) generally exceed those measured in ROMO. Figure 6 includes measurements made during FRAPPÉ at the Platteville Atmospheric Observatory (PAO), a rural location surrounded by agriculture and oil

25 and gas development (Halliday et al., 2016). Except for ethyne, observed abundances of VOCs at PAO are consistently higher

than observed at BAO. Observed abundances of VOCs both at ROMO and during the transect samples are more similar to average mixing ratios of VOCs measured in of 28 U.S. cities (Baker et al., 2008). Although measurements at ROMO were lower than most of the other locations shown in Figure 6, mixing ratios of these VOCs are much higher at ROMO than typical remote sites. Observed mixing ratios during afternoons with upslope flow can be similar to those observed simultaneously in

5   the Front Range. ROMO is a Class I area that is afforded the highest level of air quality protection, while these other locations are in major source regions. The fact that NMHC levels at ROMO are of similar magnitude to these other areas suggests a significant impact on the park from anthropogenic emissions, particularly from episodic transport.

        The ratio of i-pentane to n-pentane has been used to identify air masses impacted by oil and gas emissions. Although this ratio varies by basin, a ratio less than one is generally indicative of oil and gas emissions (COGCC, 2007; Gilman et al.,

10   2013; Prenni et al., 2016; Swarthout et al., 2013, 2015). During FRAPPÉ, Halliday et al. (2016) reported an i- to n-pentane ratio of 0.89 at the PAO, within a region of intensive oil and gas extraction activities in northeastern Colorado. This ratio is expected to be enhanced in areas where fuel evaporation is an important source of NMHCs (Harley et al., 1992; McGaughey et al., 2004), as i-pentane is an abundant component of gasoline and is elevated relative to n-pentane. As such, ratios in urban areas are often in the range of 1.5-4 (Baker et al., 2008; McLaren et al., 1996; Parrish et al., 1998; Russo et al., 2010a). For

15   ROMO-LP hourly samples, shown in Figure 7, the average ratio of i-pentane to n-pentane was 1.10 throughout the campaign. The transect samples had an average ratio of 1.19 (not shown), which is 8% higher than the ROMO hourly samples. The slightly higher values along the transects likely reflect impacts from nearby vehicle emissions. In Figure 7, markers are colored by ethane mixing ratio. As seen in Figure 7, a strong oil and gas signature is evident on many sample days, with low i- to n-pentane ratios associated with higher ethane mixing ratios; similarly, higher ratios were usually associated with lower ethane

20   mixing ratios from clean air masses transported from the west.

        Figure 8 shows the spatial and temporal variability of i- to n-pentane in all of the canister transect samples, with the points sized by ethane mixing ratio. The transect samples show a general east-west gradient with lower ratios typically observed at the easternmost sites, consistent with the oil and gas production activity in this area. However, significant variability was observed throughout the study at most of the transect sampling locations, with the range encompassing conditions indicative

25   of dominant oil and gas influence (<1), to conditions more indicative of urban influences (1.93). On three occasions samples

were collected from the Front Range up to the ROMO-TR site near the continental divide. Even limiting measurements to these three sampling dates at high elevation, the i- to n-pentane ratios indicated a range of air mass source histories impacted the park.

4. Ozone

4.1 Ozone Distributions at ROMO during FRAPPÉ

Ozone measurements at the ROMO-LP and ROMO-TR sites show coincident peaks for most of the FRAPPÉ study period (Figure 3), although O_3 mixing ratios were slightly higher and had considerably less variable at the ROMO-TR site. For ease of comparison, the frequency distributions of the O_3 mixing ratios are shown in Figure 9. The mean O_3 mixing ratios at ROMO-TR and ROMO-LP were 53 ppb (1-hr max: 82 ppb) and 43 ppb (1-hr max: 79 ppb), respectively, where ROMO-LP is lower in elevation and closer to the Front Range. Differences in these distributions can be attributed to several factors. First, the Longs Peak site is located in a valley, where pollutants can be trapped by stable nocturnal inversions, allowing efficient dry deposition or the titration of O_3 by NO, as seen by the regular nighttime decreases in O_3 in Figure 3. In comparison the Trail Ridge Road site near the Continental Divide, sits above the nocturnal inversion and is isolated from surface loss processes. This results in a skewed distribution toward lower mixing ratios at the Longs Peak site, with the median, 25th and 75th percentile values of 45 ppb, 36 ppb and 51 ppb, compared to the normal distribution at Trail Ridge Road with higher median, 25th and 75th percentile values of 53 ppb, 49 ppb and 57 ppb (Figure 9). Second, additional photochemical processing can occur during transport to the more distant Trail Ridge site during upslope events, resulting in slightly higher O_3 levels, as indicated by the 1-hr maximum values (ROMO-TR = 82 ppb; ROMO-LP = 79 ppb). Nevertheless, the relationship of the timelines of the O_3 data from both sites during elevated concentrations suggests they are often impacted by similar air masses (r^2=0.33, p<0.0001).

Elevated O_3 mixing ratios at ROMO are generally expected to be related to air masses that are transported to the site from the NRFMA resulting from the mountain-plains solenoid circulation, a local transport phenomenon occurring frequently during summertime (Bossert and Cotton, 1994; Sullivan et al., 2016; Toth and Johnson, 1985). Such conditions have the potential to transport air pollutants into the park from both oil and gas source regions, as well as urban sources across the Front Range, as shown in Figures 4 and 5. Conducting a similar back trajectory analysis for O_3 as done for the VOCs, Figure 10

shows results for HRT-ORT for the top 10% of O_3 measurements. As for the VOCs, elevated O_3 mixing ratios are largely associated with transport from the NFRMA (including Denver).

4.2 High O_3 Days

During FRAPPÉ, 1-hr O_3 mixing ratios equal to or greater than 70 ppb were observed at both the ROMO-LP and

5   ROMO-TR sites. These events are indicated by the grey shaded areas in Figure 3 and are summarized in Table 2. Elevated O_3 mixing ratios were typically accompanied by increased concentrations of various VOC source tracers. For example, alkyl nitrate concentrations (2-butyl nitrate, 2-$BuONO_2$, is shown as an example) in Figure 3 were elevated on six of the seven high O_3 days (not August 23). Alkyl nitrates are produced from the oxidation of their parent hydrocarbons such as n-butane and n-pentane, emissions derived primarily from fossil fuels in the NFRMA, and share a common photochemical production

10   mechanism with O_3. PAN was also elevated (>700 pptv) on all of the days shown in Table 2 except 23 and 24 August (see below).

VOC signatures are particularly useful in assessing the influence of oil and gas emissions in the Front Range on air masses with elevated O_3 mixing ratios transported to the park. As noted above, the i- to n-pentane ratio is expected to be less than one for air masses primarily impacted by oil and gas emissions. Two O_3 episodes, August 8 and August 18, occurred

15   when the i- to n-pentane ratios were less than one at ROMO-LP (Table 2) together with elevated levels of alkyl nitrates. As seen in Figure 3, these dates also had some of the highest ethane mixing ratios observed throughout the study period, in addition to elevated mixing ratios of halocarbons, OVOCs, and ethyne. Although the air mass VOC signature does reflect several Front Range source types, it is dominated by oil and gas emissions as evidenced in the i-pentane to n-pentane ratio.

To further investigate the impact of VOCs on O_3 we next examine photochemical products and tracers. PAN is an

20   excellent tracer of photochemical activity because it has a low background abundance and it is not directly emitted. Zaragoza et al. (2017) showed that when PAN and O_3 are disconnected in the Front Range, this indicates that the source of the O_3 is not local photochemical production. Zaragoza et al. (2017) also showed that regional mixing is common during the most photochemically active summertime days in the Front Range. Emissions from multiple sources in the region are injected into air masses as they circulate in the Front Range and secondary species reflect production driven by a mix of sources. Peak PAN

25   mixing ratios at BAO and ROMO were very similar on both August 8 and 18 (~800 pptv), supporting the assumption that

mixed Front Range air pushed up into ROMO on these particular days. PAN/PPN (propionyl peroxynitrate) ratios at BAO during the afternoon on 18 August ranged from 0.17 - 0.26. Zaragoza et al. (2017) hypothesized that these relatively high ratios are indicative of a large PAN and PPN source from the oxidation of alkanes from oil and gas production in the region, and this was recently verified by Lindaas et al. (submitted). Although PPN was not measured at ROMO, the high PAN/PPN ratio at

5 BAO, the similar PAN mixing ratios between BAO and ROMO, and the high ethane mixing ratios at ROMO together suggest important contributions from oil and gas emissions to VOC signatures and O_3 on this date. Using a series of box model simulations, Lindaas et al. (submitted)tested the sensitivity of PAN and PPN production to a large set of possible NMHC precursors observed at BAO during summer 2015, and more generally showed that propane and n-pentane are the dominant primary precursors for PPN in the Front Range.

10 We used coincident observations of alkyl nitrates during these elevated O_3 periods to estimate the contribution of the light alkane emissions to O_3 production. Alkyl nitrate formation can be used as a proxy for O_3 production if we make the following assumptions. First, their photochemical production is rapid compared to removal processes and mixing across gradients. Second, the precursor compounds (VOCs and NO_x) are collocated. Third, transport time from the source region (NFRMA) to the park is rapid (on the order of hours). For the August 8 and 18 events, the overall air mass composition (Figure

15 11) and photochemical age (Figure 12) indicate that the source region emissions and processing times in the Front Range were comparable and these assumptions are valid.

Because the production of O_3 and alkyl nitrates are tied to their common precursor, the alkyl peroxy radical (RO_2), correlation between O_3 and the C_2-C_5 alkyl nitrates is expected. Methyl nitrate is excluded from this analysis because photochemical production from its parent alkane, methane, does not meet our assumptions, and there are primary sources

20 which impact the park (Benedict et al., in review). For both of the oil and gas influenced events, O_3 is plotted against each of the alkyl nitrates for the time periods immediately before and after the event, as shown in Figure 13 for 2-butyl nitrate. This relationship can be used to provide an estimate of the excess O_3 produced resulting from the upslope events transporting oil and gas impacted air masses from the NFRMA to the park. As a first step, the y-intercept is used to estimate the background O_3 value for the event period. As shown in Table 3, each of the individual alkyl nitrates gives a slightly different background

25 O_3 value (y-intercept); however, they are all within a few ppbv of each other, providing a reasonable best estimate of the

background O$_3$ during that time period. For both events, August 8 and August 18, the average background O$_3$ was 43±2 ppbv.

This is in the range of values reported by McDuffie et al. (2016) for BAO during summer 2014.

We use these background O$_3$ values to aid in bracketing the range of influence on O$_3$ production derived from oil and

gas emissions driven by individual NMHC precursors (attributed O$_3$). To this end the orthogonal distance linear regressions

5   between O$_3$ and each of the individual C$_2$-C$_5$ alkyl nitrates are used. Table 3 provides a summary of the O$_3$/RONO$_2$ slopes in

ppbv/ppbv, intercept values (background O$_3$) in ppbv, the range of attributed O$_3$ (ppbv), and the attributed O$_3$ value (ppbv)

based on the correlation in each of the O$_3$-alkyl nitrate scatter plots. The average attributed O$_3$ production values determined

for each event are 22±3 ppbv and 19±2 ppbv for the August 8 and August 18 events at ROMO-LP, respectively. These results

are consistent with measurements along the NFRMA during FRAPPÉ by Cheadle et al. (2017), who showed that on individual

10   days emissions from oil and gas operations can contribute upwards of 30 ppbv to excess O$_3$ production. Worth noting is the

consistency of these O$_3$ enhancements for the two events and the marked similarity of the air mass compositions measured in

the park (Figure 14). Figure 14 shows O$_3$, ethane and alkyl nitrate mixing ratios during the events, along with meteorology

data. For the August 8 upslope event, the winds were variable and out of the SSE and it was sunnier (solar radiation ~200-300

W m^{-2} higher) than August 18, but ~3 °C cooler (not shown). The August 18 upslope event had winds from the east and a

15   sharp drop in solar radiation just prior to the upslope event. Nonetheless, the alkyl nitrates, light alkanes, PAN, and O$_3$ mixing

ratios were strikingly comparable during these two events (Figure 14) as were the overall air mass composition (Figure 11)

and photochemical age (Figure 12), indicating comparable source region emissions, as indicated by the dominant oil and gas

signature and the photochemical processing times.

Intermediate i- to n-pentane ratios (1.12-1.44) were observed for measurements on July 22, August 11, and August

20   12, suggesting that multiple Front Range sources impacted ROMO during these O$_3$ events. In addition to urban sources,

biomass burning emissions influenced the Front Range on August 11-12 (Dingle et al., 2016). The highest O$_3$ levels across

the Front Range during FRAPPÉ were observed on July 22 (Pfister et al., 2017; Sullivan et al., 2016), which also had the

highest average afternoon (12:00-20:00) concentrations of total alkanes (9700 pptv), alkenes (277 pptv), biogenics (252 pptv),

alkyl nitrates (110 pptv), and OVOCs (9.8 ppbv; methanol, acetaldehyde, MVK+MACR, MEK, and acetic acid) at ROMO

25   among all of the high O$_3$ days. Throughout the region, clear skies and a lower and slow growing planetary boundary layer,

coupled with reduced ventilation, resulted in less dilution and increased precursor concentrations, contributing to the elevated

O_3 (Pfister et al., 2017). These elevated mixing ratios were likely then transported to ROMO by thermally driven upslope flow

observed along the Front Range (Sullivan et al., 2016).

The O_3 events observed on August 23 (ROMO-LP) and August 24 (ROMO-TR) have neither an oil and gas nor an

5   urban signature. PAN also remained < 300 pptv during both days. Here we focus on the event on August 23 at ROMO-LP,

where VOC measurements were collocated. On August 23, air masses came from the west without passing over the NFRMA

and had much lower abundances of O_3 precursors and photochemical products (Figure 3), suggesting that the high O_3 mixing

ratios were not generated from regional photochemical production. These high O_3 mixing ratios are associated with the red

region in western Colorado in Figure 10. Mixing ratios of alkanes (total 1505 pptv), alkenes (total 93 pptv), aromatics (42

10   pptv), alkyl nitrates (total 17 ppt), halocarbons (4 pptv; C_2Cl4, CH_3I, CH_2Br_2, $CHBrCl_2$, $CHBr3$), and OVOCs (2.8 ppbv;

methanol, acetaldehyde, MVK+MACR, MEK, and acetic acid) were all low compared to the other high O_3 periods and most

of the study. For this same time period the average NO_x mixing ratio (0.52 ppbv) was lower than those during other high O_3

periods (1.2-3.1 ppbv; no data for August 11). Additionally, a comparison of soundings from Denver

(http://weather.uwyo.edu/upperair/sounding.html) shows a pocket of dry air from 500 to 100 hPa which doesn't occur on any

15   of the other high O_3 days (Figure 15a), and water vapor decreases during the event on August 23 (Figure 15b). This is the only

high O_3 event for which O_3 and water vapor exhibit a robust anti-correlation (R^2=0.627, p<0.0001) during the study. The low

coincident mixing ratios of NO_x and VOCs, the dry air aloft, and the robust anti-correlation of O_3 and water vapor at the surface

during the O_3 event suggest an intrusion of stratospheric or upper tropospheric air on August 23. A stratospheric-tropospheric

exchange event also was observed in Fort Collins in early August during FRAPPÉ (Sullivan et al., 2016).

20   **4.3 Hydroxyl Radical (OH) Reactivity and Photochemical Age**

Photolysis of NO_2 is the only way to produce O_3 in the troposphere. Oxidation of VOCs by hydroxyl radicals (OH)

in the atmosphere is typically the first step in the formation of peroxy radicals (RO_2) which react with NO to produce NO_2.

Calculating the kinetic OH reactivity (OHR) helps to identifiy compounds that are likely to quickly form RO_2 and ultimately

contribute to O_3 production. The OHR for NMHCs is calculated using the following expression:

$$OHR = \sum NMHC_i \times k_{NMHC_i+OH} \qquad \text{Eq. (1)}$$

where $[NMHC]_i$ is the concentration of each NMHC and $k_{NMHC_{i+OH}}$ is the reaction rate constant for each NMHC with OH.

The OHR is calculated for the high O_3 events during FRAPPÉ which had an oil and gas influence, a combined oil and gas and urban influence, the stratospheric/upper troposphere intrusion event, and for background conditions (without regard to the O_3 mixing ratio and defined as lowest 10th percentile for ethane). This metric is an imperfect measure of O_3 production potential

5 since it does not account for chain termination or propagation steps, nor does it properly capture differences in VOC production of peroxy radicals during photolysis or reaction with other oxidants. However, OHR is a useful tool because it is a measure of the initial rate of peroxy radical formation that can be interpreted as the potential for a specific compound to ultimately produce O_3.

  For the events influenced by oil and gas emissions, the alkanes were the major contributor to the NMHC-OHR,

10 comprising almost 70% of the calculated total (Figure 11). For the high O_3 air masses that also included an urban influence, the OHR for alkenes (~28%) and alkanes (~37%) were more comparable, reflecting increased reactivity contributions of the light alkenes from urban areas. However, the alkanes were still the largest contributor of OH reactivity to this category. The importance of isoprene, with ~32% of the total reactivity, is also more apparent, even though the average mixing ratio was only 64 pptv for these days. Interestingly, the overall background NMHC-OHR (0.86 s^{-1}) was comparable to that of the oil

15 and gas influenced days (0.90 s^{-1} OHR). Larger mixing ratios of isoprene (~270 pptv) during background periods results in the calculated NMHC-OHR being dominated (~86%) by isoprene reactivity and of similar magnitutude as the more polluted oil and gas days. In all cases, ethyne and the aromatics were only minor contributors to the calculated overall OHR. Finally, it is worth noting that the OHR values calculated here are lower bounds on the actual VOC-OHR in the studied air masses. The OHR values only represent the initial attack of OH with the NMHC and does not consider the subsequent contributions

20 of the oxidation products formed and how these influence and change the overall air mass and its reactivity. As Abeleira et al. (2017) points out for measurements at BAO, other VOC classes not included in the ROMO analysis (e.g., oxygenated VOCs) are also significant contributors to total VOC-OHR.

  To estimate the impact of the oil and gas emissions on OHR at the park, we compare the average straight chain alkane OHR during the upslope events to that of the background and combined oil and gas and urban-influenced alkane OHRs, which

25 include the C_2-C_8 alkanes. The reactivity attributed to the alkanes is considered because they are the dominant VOCs associated

with the oil and gas emissions. The alkane OHR for the oil and gas events was 0.62 s⁻¹, which comprised ~70% of the total calculated OHR (includes all measured compounds) for those events. In comparison to the oil and gas influenced events, the alkane OHR for the urban-influenced events was only 0.21 s⁻¹, while the background alkane OHR was only 0.02 s⁻¹, and comprised much smaller fractions of the total calculated OHR for those periods. The difference in alkane reactiviy between

5   the oil and gas events and the urban-influenced events was 0.41 s⁻¹; the difference between oil and gas influenced and background events was 0.60 s⁻¹. Furthermore, the percent contribution of the individual straight chain C_2-C_8 alkanes to the total alkane OHR is similar to that of other measurements made in the regions across seasons (Abeleira et al., 2017; Halliday et al., 2016; McDuffie et al., 2016; Swarthout et al., 2013) underscoring the consistent temporal and spatial compositional influence of the oil and gas source signature impacting ROMO during upslope events (Table 4).

10   Air mass photochemical age can be calculated using the alkyl nitrate to parent hydrocarbon ratio (R-ONO₂/R-H) (e.g. Bertman et al., 1995; Russo et al., 2010b; Simpson et al., 2003; Swarthout et al., 2013). This reaction scheme assumes only OH-initiated photochemical production of a given alkyl nitrate from its parent hydrocarbon, and so deviations from the model suggest additional sources or chemistry not captured in this simple scheme. Details of the chemical mechanisms and calculations can be found in the supplement. The modeled ratios of 3-pentyl nitrate to n-pentane versus 2-butyl nitrate to n-

15   butane are calculated using [OH] = 10^6 molecules cm⁻³ and are shown as the solid line in Figure 12. Measured ratios of these species are shown as the symbols and are colored by O₃ mixing ratio. Based on this model, VOC ages in sampled air masses ranged from several hours to two days and, as generally observed with the pentyl nitrates, they typically lie below the model prediction line with a relatively small offset. Focusing on the high O₃ periods, shown as red filled symbols, the oil and gas influenced events on August 8 and August 18 show the best agreement with the model, with a photochemical age of less than

20   one day, indicating local sources of the parent hydrocarbons and that photochemical production was driving the O₃ and alkyl nitrate production these days. On July 22, August 11 and August 12, when both urban and oil and gas impacts were observed, the measured ratios deviate from the model in a systematic way, suggesting that the air masses were influenced by multiple chemical processes. Finally, on August 23 and 24, the alkyl nitrate to parent alkane ratios deviated from the photochemical line significantly, providing another line of evidence that the increase in O₃ was not from photochemical production in a

25   polluted environment, consistent with influences of O₃ enriched air from the upper troposphere.

5. Summary and Conclusions

Rocky Mountain National Park is a Class I area that is afforded the highest level of air quality protection. Nevertheless, O_3 mixing ratios can reach levels that negatively impact vegetation and human health, particularly for older adults and people who are active outdoors. In this study, O_3 and a suite of VOC measurements were made at ROMO as part

5 of the 2014 FRAPPÉ field campaign. Although average and peak O_3 mixing ratios were lower during FRAPPÉ compared to other recent summer seasons, one-hour mixing ratios exceeding 70 ppbv routinely measured in the park during this period. This study was aimed at better understanding sources of VOCs that impact the park and, particularly, what drives these high ozone events.

ROMO is located just west of the NFRMA in Colorado, and the park can be impacted by a variety of emissions

10 sources. Significant variability in the measured VOC abundances suggest that the sampling site was impacted by emissions from biogenic, urban, combustion, agricultural, and oil and gas sources during the study period. Light alkanes measured at ROMO, markers for oil and gas production, were significantly elevated relative to background levels, and at times reached mixing ratios measured in some oil and gas source regions during upslope events (e.g., Swarthout et al, 2015). Mixing ratios reached 9800 ppt for ethane, 1158 ppt for i-butane, 2378 ppt for n-butane, 2095 ppt for i-pentane, and 1712 ppt for n-pentane.

15 Using VOCs as source markers, we determined that the elevated O_3 periods were primarily associated with upslope events. For the oil and gas impacted days, light alkanes contributed approximately 20 ppbv excess O_3, having a major impact on total O_3 mixing ratios on those days. In air masses with increased urban influence, alkenes played a more important role; however, even for these urban influenced air masses, a clear oil and gas signature was also present. During background periods, when air masses arrived from the west, O_3 was typically low and NMHC -OH reactivity was dominated by isoprene (86%). Total

20 NMHC-OHR was of similar magntitude on the background (0.86 s^{-1}) and oil and gas influenced (0.895 s^{-1}) days but alkanes dominated total NMHC-OHR (69%) on oil and gas days. The mixed urban and oil and gas influenced days were characterized by slightly lower total NMHC-OHR (0.546 s^{-1}) and OH reactivity was dominated by alkanes (37%) and alkenes (28%). In one distinct case, elevated O_3 was associated with air mass transport from the west. For this case, the abundances of VOCs and other secondary species were very low (Total NMHC-OHR =0.07s^{-1}), and there was a clear anti-correlation of O_3 and surface

water vapor, suggesting that an intrusion of stratospheric or O_3-rich upper-tropospheric air contributed to elevated O_3 measured at the surface.

Elevated O_3 in the Front Range and ROMO has been a persistent air quality issue. Findings from this study reaffirm that ROMO is impacted by a variety of anthropogenic emissions sources in the NFRMA. State and federal agencies have implemented regulations that have successfully reduced emissions from traditional sources (mobile, power plant, and other activities) gradually reducing O_3 since 2009 at a rate of -0.25 ± 0.13 ppbv yr^{-1} in ROMO (McGlynn et al., 2018). Continued population growth and the competing effects of increasing emissions from oil and gas extraction appear to be diminishing the impact of the regulations as emissions from emerging sectors or increased population are contributing to the high O_3 episodes. Management practices aimed at reducing high O_3 levels at the park thus cannot focus on controlling a single source, but instead must take a broader approach to focus on reductions in the traditional sources as well as these new sources. Recent work by Zhou et al. (in prep) suggest that emission reductions of both volatile organic compounds (VOCs) and nitrogen oxides (NO$_x$) could lead to effective O_3 mitigation in the Intermountain West. Additionally, identifying periods of stratospheric O_3 influence should also be a priority when assessing which high O_3 episodes can be mitigated through emissions control.

Data Availability

The data used in this analysis are available in the FRAPPÉ/DISCOVER-AQ data archive (https://www-air.larc.nasa.gov/cgi-bin/ArcView/discover-aq.co-2014) in the Ground-Other category under the PIs Collett, Fischer, and Sive.

Acknowledgements

Support for this work was provided by the National Park Service. The assumptions, findings, conclusions, judgments, and views presented herein are those of the authors and should not be interpreted as necessarily representing the National Park Service.

References

Abeleira, A., Pollack, I. B., Sive, B., Zhou, Y., Fischer, E. V. and Farmer, D. K.: Source characterization of volatile organic compounds in the Colorado Northern Front Range Metropolitan Area during spring and summer 2015, J. Geophys. Res. Atmospheres, 122(6), 2016JD026227, doi:10.1002/2016JD026227, 2017.

5 Ashbaugh, L. L., Malm, W. C. and Sadeh, W. Z.: A residence time probability analysis of sulfur concentrations at Grand Canyon National Park, Atmospheric Environ. 1967, 19(8), 1263–1270, doi:10.1016/0004-6981(85)90256-2, 1985.

Atkinson, R.: Kinetics and mechanisms of the gas-phase reactions of the hydroxyl radical with organic compounds under atmospheric conditions, Chem. Rev., 86(1), 69–201, doi:10.1021/cr00071a004, 1986.

Atkinson, R. and Arey, J.: Atmospheric Degradation of Volatile Organic Compounds, Chem. Rev., 103(12), 4605–4638,
10 doi:10.1021/cr0206420, 2003.

Baker, A. K., Beyersdorf, A. J., Doezema, L. A., Katzenstein, A., Meinardi, S., Simpson, I. J., Blake, D. R. and Sherwood Rowland, F.: Measurements of nonmethane hydrocarbons in 28 United States cities, Atmos. Environ., 42(1), 170–182, doi:10.1016/j.atmosenv.2007.09.007, 2008.

Beem, K. B., Raja, S., Schwandner, F. M., Taylor, C., Lee, T., Sullivan, A. P., Carrico, C. M., McMeeking, G. R., Day, D.,
15 Levin, E., Hand, J., Kreidenweis, S. M., Schichtel, B., Malm, W. C. and Collett, J. L.: Deposition of reactive nitrogen during the Rocky Mountain Airborne Nitrogen and Sulfur (RoMANS) study, Environ. Pollut., 158(3), 862–872, doi:10.1016/j.envpol.2009.09.023, 2010.

Benedict, K. B., Prenni, A. J., Sullivan, A. P., Evanoski-Cole, A. R., Fischer, E. V., Callahan, S., Sive, B. C., Zhou, Y., Schichtel, B. A. and Collett Jr., J. L.: Impact of Front Range Sources on Reactive Nitrogen Concentrations and Deposition in
20 Rocky Mountain National Park, PeerJ, in review.

Benedict, K. B., Day, D., Schwandner, F. M., Kreidenweis, S. M., Schichtel, B., Malm, W. C. and Collett, J. L.: Observations of atmospheric reactive nitrogen species in Rocky Mountain National Park and across northern Colorado, Atmos. Environ., 64, 66–76, doi:10.1016/j.atmosenv.2012.08.066, 2013.

Bertman, S. B., Roberts, J. M., Parrish, D. D., Buhr, M. P., Goldan, P. D., Kuster, W. C., Fehsenfeld, F. C., Montzka, S. A.
25 and Westberg, H.: Evolution of alkyl nitrates with air mass age, J. Geophys. Res. Atmospheres, 100(D11), 22805–22813, doi:10.1029/95JD02030, 1995.

Blake, D. R., Blake, N. J., Smith, T. W., Wingenter, O. W. and Rowland, F. S.: Nonmethane hydrocarbon and halocarbon distributions during Atlantic Stratocumulus Transition Experiment/Marine Aerosol and Gas Exchange, June 1992, J. Geophys. Res. Atmospheres, 101(D2), 4501–4514, doi:10.1029/95JD01370, 1996.

30 Bossert, J. E. and Cotton, W. R.: Regional-Scale Flows in Mountainous Terrain. Part I: A Numerical and Observational Comparison, Mon. Weather Rev., 122(7), 1449–1471, doi:10.1175/1520-0493(1994)122<1449:RSFIMT>2.0.CO;2, 1994.

Cheadle, L. C., Oltmans, S. J., Petron, G., Schnell, R. C., Mattson, E. J., Herndon, S. C., Thompson, A. M., Blake, D. R. and McClure-Begley, A.: Surface ozone in the Colorado northern Front Range and the influence of oil and gas development during FRAPPE/DISCOVER-AQ in summer 2014, Elem Sci Anth, 5(0), doi:10.1525/elementa.254, 2017.

Christensen, J. N., Weiss-Penzias, P., Fine, R., McDade, C. E., Trzepla, K., Brown, S. T. and Gustin, M. S.: Unraveling the sources of ground level ozone in the Intermountain Western United States using Pb isotopes, Sci. Total Environ., 530–531, 519–525, doi:10.1016/j.scitotenv.2015.04.054, 2015.

COGCC: Greater Wattenberg Area Baseline Study, Technical Report, Colorado Oil and Gas Conservation Commission., 2007.

COGCC: Well Surface Location Data, CO Oil and Gas Conservation Commission. [online] Available from: http://cogcc.state.co.us/data2.html#/downloads (Accessed 24 January 2018), 2018.

Dingle, J. H., Vu, K., Bahreini, R., Apel, E. C., Campos, T. L., Flocke, F., Fried, A., Herndon, S., Hills, A. J., Hornbrook, R. S., Huey, G., Kaser, L., Montzka, D. D., Nowak, J. B., Reeves, M., Richter, D., Roscioli, J. R., Shertz, S., Stell, M., Tanner, D., Tyndall, G., Walega, J., Weibring, P. and Weinheimer, A.: Aerosol optical extinction during the Front Range Air Pollution and Photochemistry Éxperiment (FRAPPÉ) 2014 summertime field campaign, Colorado, USA, Atmospheric Chem. Phys., 16(17), 11207–11217, doi:10.5194/acp-16-11207-2016, 2016.

Gebhart, K. A., Schichtel, B. A., Malm, W. C., Barna, M. G., Rodriguez, M. A. and Collett, J. L.: Back-trajectory-based source apportionment of airborne sulfur and nitrogen concentrations at Rocky Mountain National Park, Colorado, USA, Atmos. Environ., 45(3), 621–633, doi:10.1016/j.atmosenv.2010.10.035, 2011.

Gebhart, K. A., Malm, W. C., Rodriguez, M. A., Barna, M. G., Schichtel, B. A., Benedict, K. B., Collett, J. L. and Carrico, C. M.: Meteorological and Back Trajectory Modeling for the Rocky Mountain Atmospheric Nitrogen and Sulfur Study II, Adv. Meteorol., 2014, 1–19, doi:10.1155/2014/414015, 2014.

Gilman, J. B., Lerner, B. M., Kuster, W. C. and de Gouw, J. A.: Source Signature of Volatile Organic Compounds from Oil and Natural Gas Operations in Northeastern Colorado, Environ. Sci. Technol., 47(3), 1297–1305, doi:10.1021/es304119a, 2013.

Halliday, H. S., Thompson, A. M., Wisthaler, A., Blake, D. R., Hornbrook, R. S., Mikoviny, T., Müller, M., Eichler, P., Apel, E. C. and Hills, A. J.: Atmospheric benzene observations from oil and gas production in the Denver-Julesburg Basin in July and August 2014, J. Geophys. Res. Atmospheres, 121(18), 2016JD025327, doi:10.1002/2016JD025327, 2016.

Harley, R. A., Hannigan, M. P. and Cass, G. R.: Respeciation of organic gas emissions and the detection of excess unburned gasoline in the atmosphere, Environ. Sci. Technol., 26(12), 2395–2408, doi:10.1021/es00036a010, 1992.

Janjic, Z. I.: A nonhydrostatic model based on a new approach, Meteorol. Atmospheric Phys., 82(1–4), 271–285, doi:10.1007/s00703-001-0587-6, 2003.

Kohut, R., Flanagan, C., Cheatham, J. and Porter, E.: Foliar Ozone Injury on Cutleaf Coneflower at Rocky Mountain National Park, Colorado, West. North Am. Nat., 72(1), 32–42, doi:10.3398/064.072.0104, 2012.

Koppmann, R., Ed.: Volatile Organic Compounds in the Atmosphere, 1 edition., Wiley-Blackwell, Oxford ; Ames, Iowa., 2007.

Lin, M., Fiore, A. M., Horowitz, L. W., Langford, A. O., Oltmans, S. J., Tarasick, D. and Rieder, H. E.: Climate variability modulates western US ozone air quality in spring via deep stratospheric intrusions, Nat. Commun., 6, 7105, doi:10.1038/ncomms8105, 2015.

Lindaas, J., Farmer, D. K., Pollack, I. B., Abeleira, A., Flocke, F. and Fischer, E. V.: Acyl peroxy nitrates link oil and natural
5   gas emissions to high ozone abundances in the Colorado Front Range during summer 2015, J. Geophys. Res.-Atmospheres, submitted.

McDuffie, E. E., Edwards, P. M., Gilman, J. B., Lerner, B. M., Dubé, W. P., Trainer, M., Wolfe, D. E., Angevine, W. M., deGouw, J., Williams, E. J., Tevlin, A. G., Murphy, J. G., Fischer, E. V., McKeen, S., Ryerson, T. B., Peischl, J., Holloway, J. S., Aikin, K., Langford, A. O., Senff, C. J., Alvarez, R. J., Hall, S. R., Ullmann, K., Lantz, K. O. and Brown, S. S.: Influence
10   of oil and gas emissions on summertime ozone in the Colorado Northern Front Range, J. Geophys. Res. Atmospheres, 121(14), 2016JD025265, doi:10.1002/2016JD025265, 2016.

McGaughey, G. R., Desai, N. R., Allen, D. T., Seila, R. L., Lonneman, W. A., Fraser, M. P., Harley, R. A., Pollack, A. K., Ivy, J. M. and Price, J. H.: Analysis of motor vehicle emissions in a Houston tunnel during the Texas Air Quality Study 2000, Atmos. Environ., 38(20), 3363–3372, doi:10.1016/j.atmosenv.2004.03.006, 2004.

15   McGlynn, D., Mao, H., Wu, Z., Sive, B. and Sharac, T.: Understanding Long-Term Variations in Surface Ozone in United States (U.S.) National Parks, Atmosphere, 9(4), 125, doi:10.3390/atmos9040125, 2018.

McLaren, R., Singleton, D. L., Lai, J. Y. K., Khouw, B., Singer, E., Wu, Z. and Niki, H.: Analysis of motor vehicle sources and their contribution to ambient hydrocarbon distributions at urban sites in Toronto during the Southern Ontario oxidants study, Atmos. Environ., 30(12), 2219–2232, doi:10.1016/1352-2310(95)00178-6, 1996.

20   Musselman, R. C. and Korfmacher, J. L.: Ozone in remote areas of the Southern Rocky Mountains, Atmos. Environ., 82, 383–390, doi:10.1016/j.atmosenv.2013.10.051, 2014.

National Park Service: Stats Report Viewer, [online] Available from: https://irma.nps.gov/Stat/Reports/Park (Accessed 3 February 2017), 2017.

Parrish, D. D., Trainer, M., Young, V., Goldan, P. D., Kuster, W. C., Jobson, B. T., Fehsenfeld, F. C., Lonneman, W. A., Zika,
25   R. D., Farmer, C. T., Riemer, D. D. and Rodgers, M. O.: Internal consistency tests for evaluation of measurements of anthropogenic hydrocarbons in the troposphere, J. Geophys. Res. Atmospheres, 103(D17), 22339–22359, doi:10.1029/98JD01364, 1998.

Pétron, G., Frost, G., Miller, B. R., Hirsch, A. I., Montzka, S. A., Karion, A., Trainer, M., Sweeney, C., Andrews, A. E., Miller, L., Kofler, J., Bar-Ilan, A., Dlugokencky, E. J., Patrick, L., Moore, C. T., Ryerson, T. B., Siso, C., Kolodzey, W., Lang, P. M.,
30   Conway, T., Novelli, P., Masarie, K., Hall, B., Guenther, D., Kitzis, D., Miller, J., Welsh, D., Wolfe, D., Neff, W. and Tans, P.: Hydrocarbon emissions characterization in the Colorado Front Range: A pilot study, J. Geophys. Res. Atmospheres, 117(D4), D04304, doi:10.1029/2011JD016360, 2012.

Pfister, G. G., Reddy, P. J., Barth, M. C., Flocke, F. F., Fried, A., Herndon, S. C., Sive, B. C., Sullivan, J. T., Thompson, A. M., Yacovitch, T. I., Weinheimer, A. J. and Wisthaler, A.: Using Observations and Source-Specific Model Tracers to

Characterize Pollutant Transport During FRAPPÉ and DISCOVER-AQ, J. Geophys. Res. Atmospheres, 122(19), 2017JD027257, doi:10.1002/2017JD027257, 2017.

Poirot, R. L., Wishinski, P. R., Hopke, P. K. and Polissar, A. V.: Comparative Application of Multiple Receptor Methods To Identify Aerosol Sources in Northern Vermont, Environ. Sci. Technol., 35(23), 4622–4636, doi:10.1021/es010588p, 2001.

Prenni, A. J., Day, D. E., Evanoski-Cole, A. R., Sive, B. C., Hecobian, A., Zhou, Y., Gebhart, K. A., Hand, J. L., Sullivan, A. P., Li, Y., Schurman, M. I., Desyaterik, Y., Malm, W. C., Collett Jr., J. L. and Schichtel, B. A.: Oil and gas impacts on air quality in federal lands in the Bakken region: an overview of the Bakken Air Quality Study and first results, Atmos Chem Phys, 16(3), 1401–1416, doi:10.5194/acp-16-1401-2016, 2016.

Reddy, P. J. and Pfister, G. G.: Meteorological factors contributing to the interannual variability of midsummer surface ozone in Colorado, Utah, and other western U.S. states, J. Geophys. Res. Atmospheres, 121(5), 2015JD023840, doi:10.1002/2015JD023840, 2016.

Russo, R. S., Zhou, Y., White, M. L., Mao, H., Talbot, R. and Sive, B. C.: Multi-year (2004–2008) record of nonmethane hydrocarbons and halocarbons in New England: seasonal variations and regional sources, Atmos Chem Phys, 10(10), 4909–4929, doi:10.5194/acp-10-4909-2010, 2010a.

Russo, R. S., Zhou, Y., Haase, K. B., Wingenter, O. W., Frinak, E. K., Mao, H., Talbot, R. W. and Sive, B. C.: Temporal variability, sources, and sinks of C1-C5 alkyl nitrates in coastal New England, Atmos Chem Phys, 10(4), 1865–1883, doi:10.5194/acp-10-1865-2010, 2010b.

Simpson, I. J., Blake, N. J., Blake, D. R., Atlas, E., Flocke, F., Crawford, J. H., Fuelberg, H. E., Kiley, C. M., Meinardi, S. and Rowland, F. S.: Photochemical production and evolution of selected C2–C5 alkyl nitrates in tropospheric air influenced by Asian outflow, J. Geophys. Res. Atmospheres, 108(D20), 8808, doi:10.1029/2002JD002830, 2003.

Sive, B. C.: Atmospheric Nonmethane Hydrocarbons: Analytical Methods and Estimated Hydroxyl Radical Concentrations, University of California, Irvine., 1998.

Sive, B. C., Zhou, Y., Troop, D., Wang, Y., Little, W. C., Wingenter, O. W., Russo, R. S., Varner, R. K. and Talbot, R.: Development of a Cryogen-Free Concentration System for Measurements of Volatile Organic Compounds, Anal. Chem., 77(21), 6989–6998, doi:10.1021/ac0506231, 2005.

Stein, A. F., Draxler, R. R., Rolph, G. D., Stunder, B. J. B., Cohen, M. D. and Ngan, F.: NOAA's HYSPLIT Atmospheric Transport and Dispersion Modeling System, Bull. Am. Meteorol. Soc., 96(12), 2059–2077, doi:10.1175/BAMS-D-14-00110.1, 2015.

Strode, S. A., Rodriguez, J. M., Logan, J. A., Cooper, O. R., Witte, J. C., Lamsal, L. N., Damon, M., Van Aartsen, B., Steenrod, S. D. and Strahan, S. E.: Trends and variability in surface ozone over the United States, J. Geophys. Res. Atmospheres, 120(17), 2014JD022784, doi:10.1002/2014JD022784, 2015.

Sullivan, J. T., McGee, T. J., Langford, A. O., Alvarez, R. J., Senff, C. J., Reddy, P. J., Thompson, A. M., Twigg, L. W., Sumnicht, G. K., Lee, P., Weinheimer, A., Knote, C., Long, R. W. and Hoff, R. M.: Quantifying the contribution of thermally

driven recirculation to a high-ozone event along the Colorado Front Range using lidar, J. Geophys. Res. Atmospheres, 2016JD025229, doi:10.1002/2016JD025229, 2016.

Swarthout, R. F., Russo, R. S., Zhou, Y., Hart, A. H. and Sive, B. C.: Volatile organic compound distributions during the NACHTT campaign at the Boulder Atmospheric Observatory: Influence of urban and natural gas sources, J. Geophys. Res. Atmospheres, 118(18), 10,614-10,637, doi:10.1002/jgrd.50722, 2013.

Swarthout, R. F., Russo, R. S., Zhou, Y., Miller, B. M., Mitchell, B., Horsman, E., Lipsky, E., McCabe, D. C., Baum, E. and Sive, B. C.: Impact of Marcellus Shale Natural Gas Development in Southwest Pennsylvania on Volatile Organic Compound Emissions and Regional Air Quality, Environ. Sci. Technol., 49(5), 3175–3184, doi:10.1021/es504315f, 2015.

Toth, J. and Johnson, R.: Summer Surface Flow Characteristics Over Northeast Colorado, Mon. Weather Rev., 113(9), 1458–1469, doi:10.1175/1520-0493(1985)113<1458:SSFCON>2.0.CO;2, 1985.

Tzompa-Sosa, Z. A., Mahieu, E., Franco, B., Keller, C. A., Turner, A. J., Helmig, D., Fried, A., Richter, D., Weibring, P., Walega, J., Yacovitch, T. I., Herndon, S. C., Blake, D. R., Hase, F., Hannigan, J. W., Conway, S., Strong, K., Schneider, M. and Fischer, E. V.: Revisiting global fossil fuel and biofuel emissions of ethane, J. Geophys. Res. Atmospheres, 122(4), 2016JD025767, doi:10.1002/2016JD025767, 2017.

Wooldridge, G., Zeller, K. and Musselman, R.: Ozone concentration characteristics at a high-elevation forest site, Theor. Appl. Climatol., 56(3–4), 153–164, doi:10.1007/BF00866424, 1997.

Zaragoza, J., Callahan, S., McDuffie, E. E., Kirkland, J., Brophy, P., Durrett, L., Farmer, D. K., Zhou, Y., Sive, B., Flocke, F., Pfister, G., Knote, C., Tevlin, A., Murphy, J. and Fischer, E. V.: Observations of acyl peroxy nitrates during the Front Range Air Pollution and Photochemistry Éxperiment (FRAPPÉ), J. Geophys. Res. Atmospheres, 2017JD027337, doi:10.1002/2017JD027337, 2017.

Zhou, Y., Mao, H. and Sive, B. C.: Impacts of Oil and Gas Emissions on Long-term Trends in Surface Ozone in the Intermountain West National Parks During 2005 – 2015, in prep, in prep.

Zhou, Y., Shively, D., Mao, H., Russo, R. S., Pape, B., Mower, R. N., Talbot, R. and Sive, B. C.: Air Toxic Emissions from Snowmobiles in Yellowstone National Park, Environ. Sci. Technol., 44(1), 222–228, doi:10.1021/es9018578, 2010.
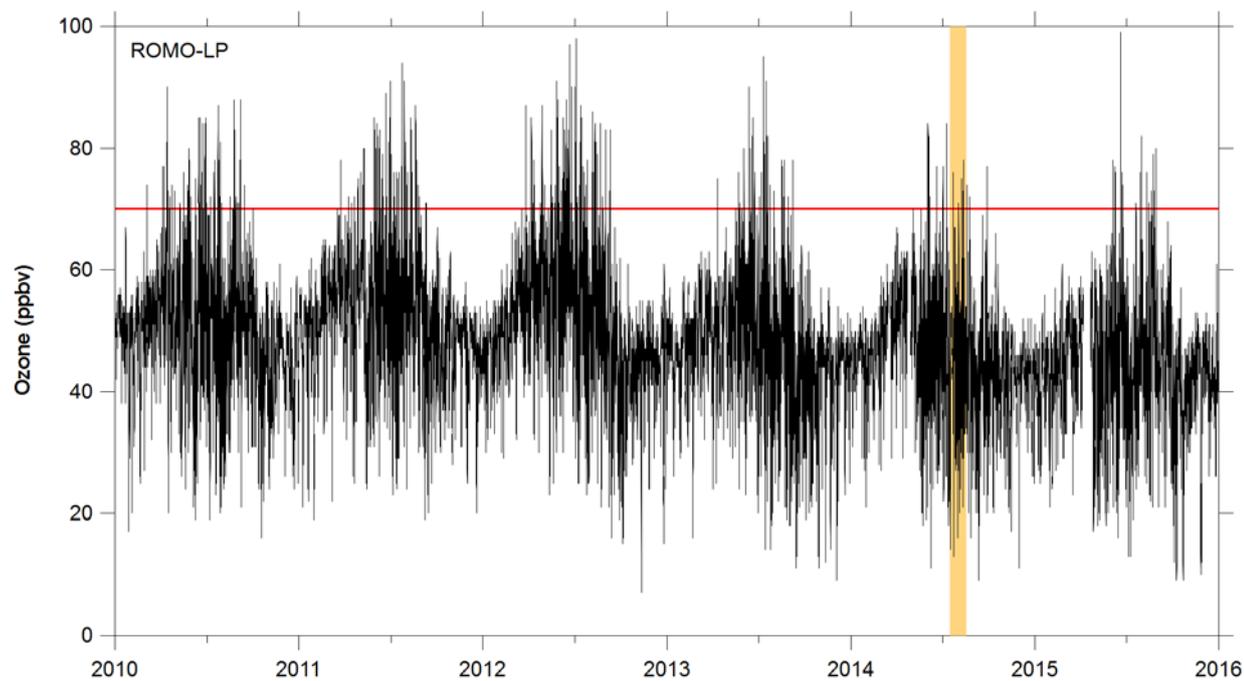
Figure 1. Hourly O₃ measurements at ROMO-LP from January 2010 to December 2015. The red line indicates the current NAAQS 8-hr daily maximum value of 70 ppb. The shaded region designates the FRAPPÉ study period.
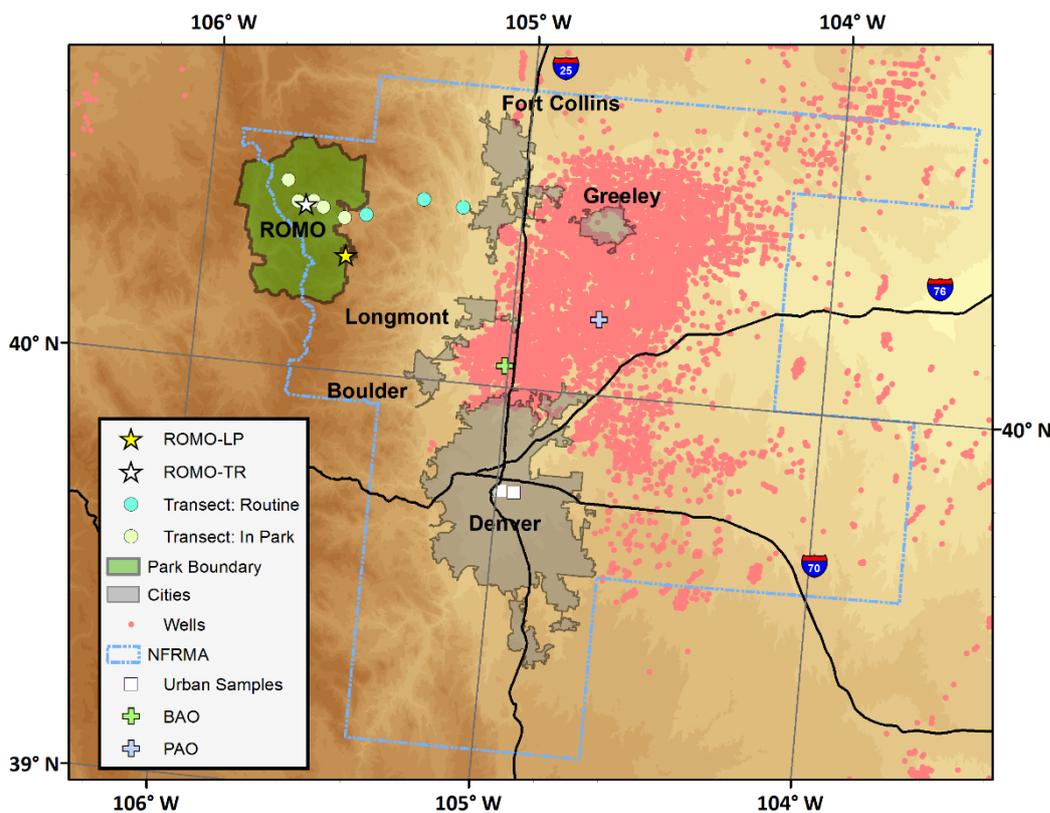
Figure 2. Map of sampling sites, including locations of the transect samples. Also shown are oil and gas well locations (COGCC, 2018) and cities along the NFRMA.
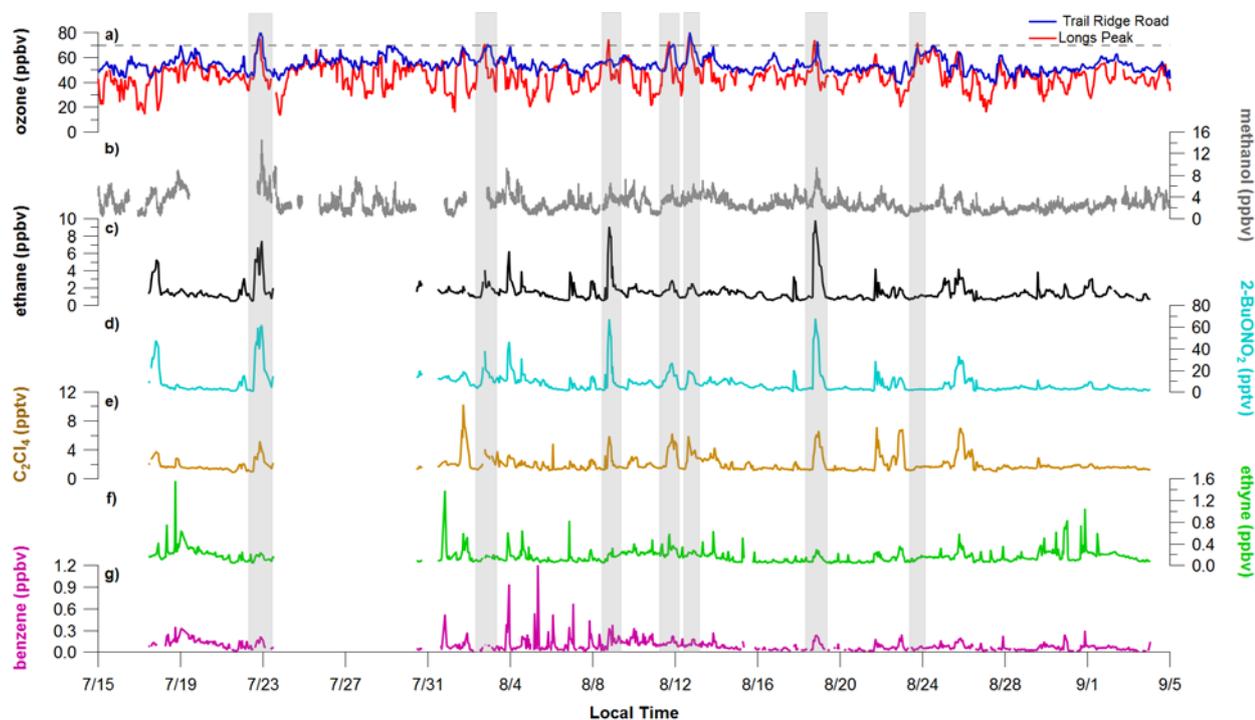
Figure 3. A subset of VOCs measured at the ROMO-LP site from 17 July to 4 September 2014. From 19-22 and 23-30 July, the PTR-MS and GC system, respectively, were shut down due to air conditioner failures in the field laboratories. Ozone measurements from both the ROMO-LP (Longs Peak) and ROMO-TR (Trail Ridge Road) sites are also shown. Shaded areas represent periods selected for further analysis when hourly O$_3$ exceeded 70 ppb (dashed line).
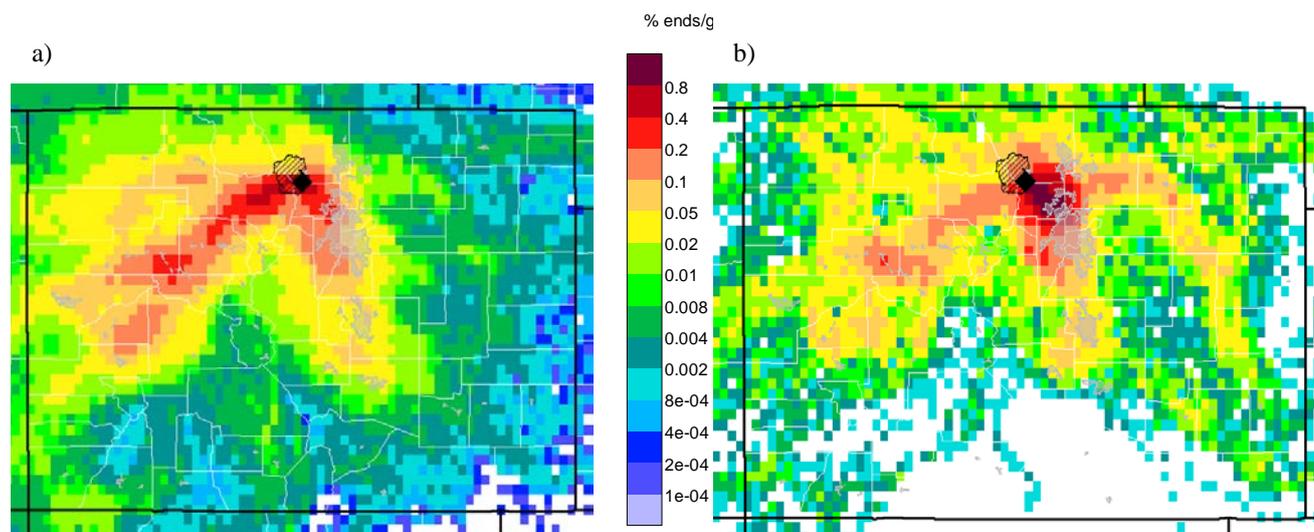
5 **Figure 4. Residence time maps showing areas up to 2 days upwind of ROMO-LP (black diamond) during (a) all hours of the study period (July 17 – Sept 4, 2014) and (b) during hours with ethane > 90th percentile. Colors indicate the relative frequency of transport. Light gray overlay indicated urban areas.**
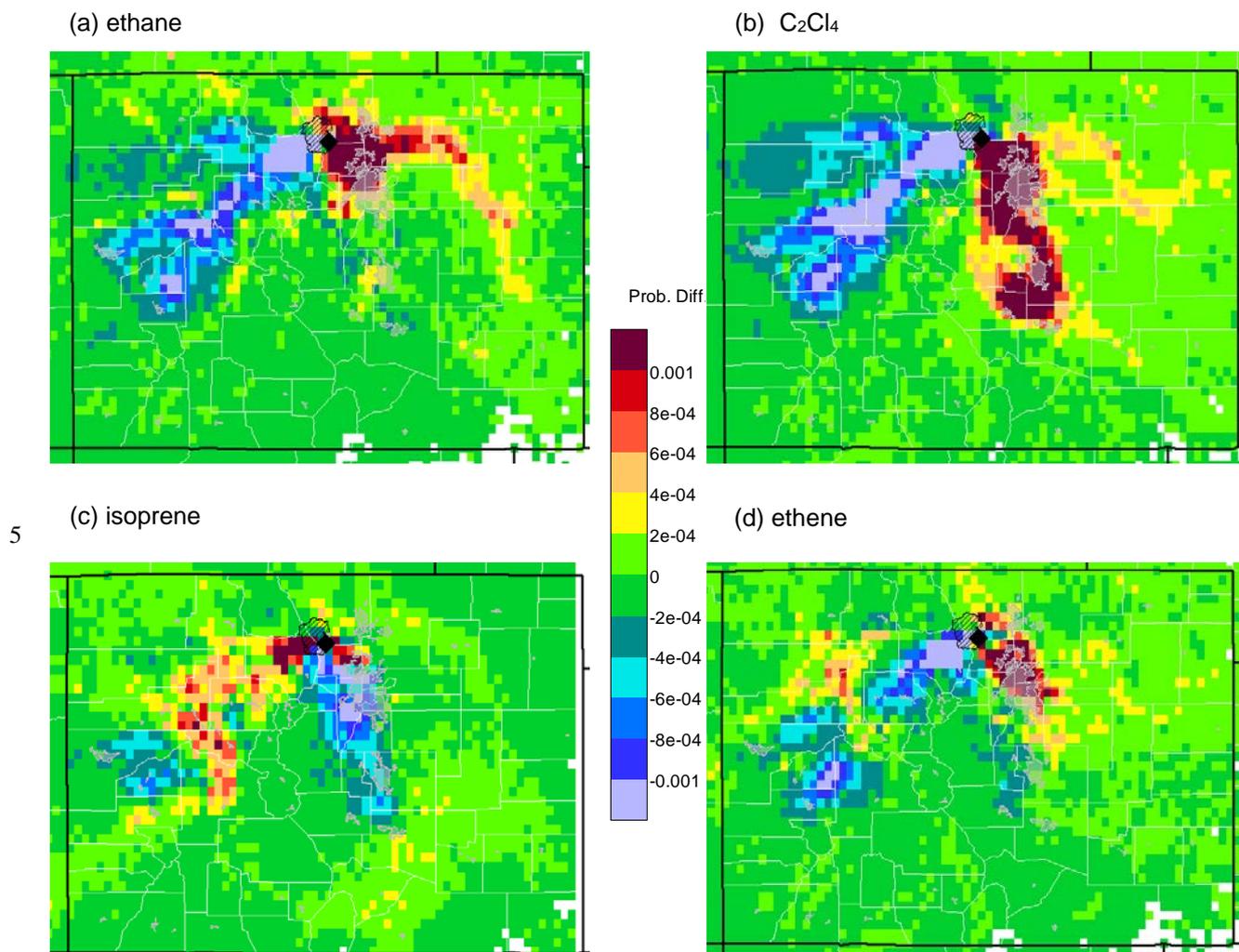
Figure 5. Differences between upwind transport during hours of 90th percentile or higher mixing ratios and average conditions during the study (HRT-ORT) for (a) ethane, (b) C₂Cl₄, (c) isoprene, and (d) ethene. Yellow to red colors indicate areas that were more likely than average to be upwind during the 2 days prior to a high concentration measurement at ROMO-LP (black diamond). Blue to purple colors indicate areas that were less likely to be upwind, while areas in green had similar likelihoods of being upwind during average hours and during high mixing ratio hours. Light gray overlay indicated urban areas.
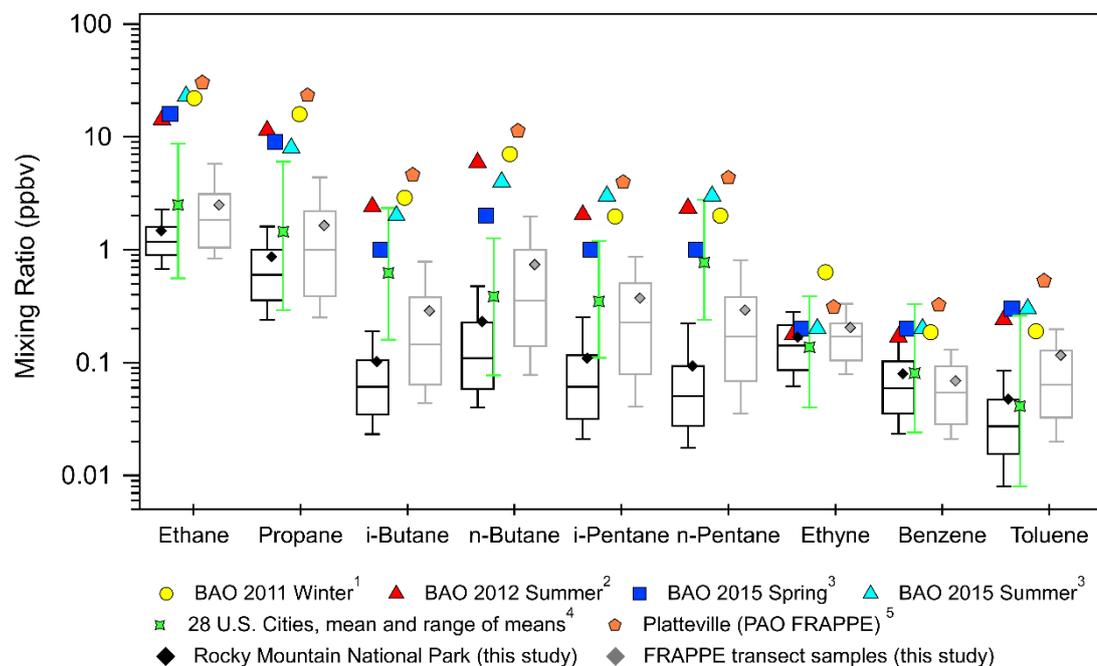
Figure 6. Box plots for mixing ratios of selected VOCs in ROMO hourly samples (black) and all transect canister samples (gray) and mean mixing ratios from previous studies ([1]Swarthout et al. (2013), [2]McDuffie et al. (2016) [3]Abeleria et al. (2017), [4] Baker et al. (2008), [5] Halliday et al. (2016)). Median mixing ratios from this study are shown as the black horizontal lines and the means are shown as the diamond symbols.
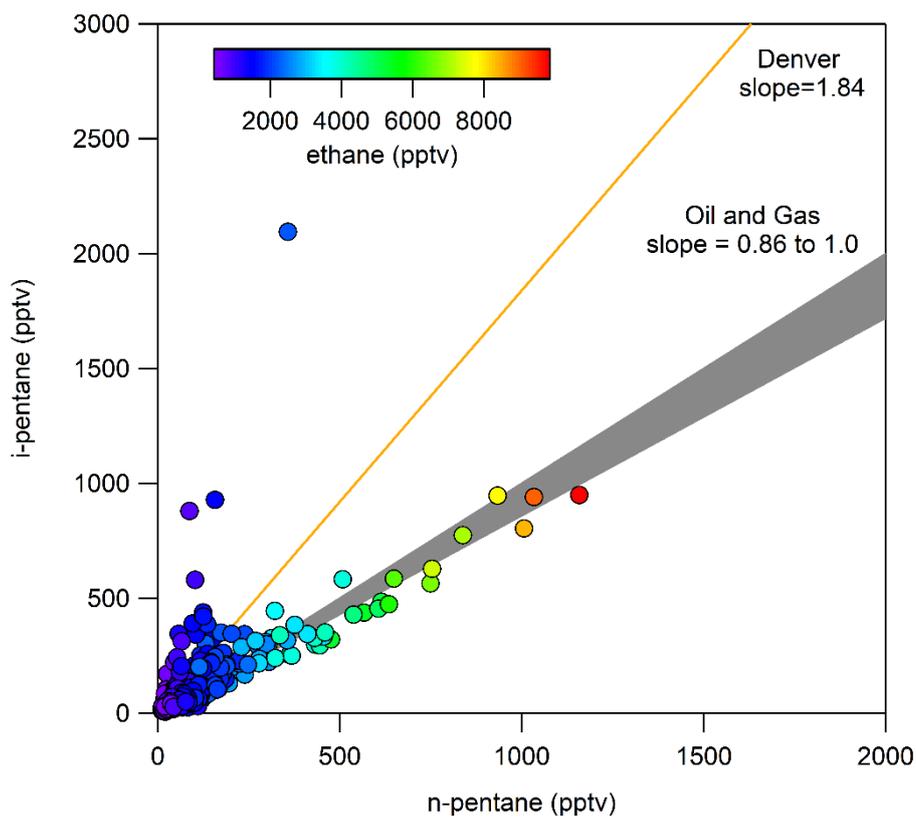
Figure 7. Iso-pentane versus n-pentane for ROMO hourly samples, colored by ethane mixing ratio. For reference, also shown are the i- to n-pentane ratio for measurements collected in Denver (Baker et al., 2008) and a range of slopes from 0.86 to 1 line where everything that falls in this range indicates oil and gas influenced (COGCC, 2007; Gilman et al., 2013).
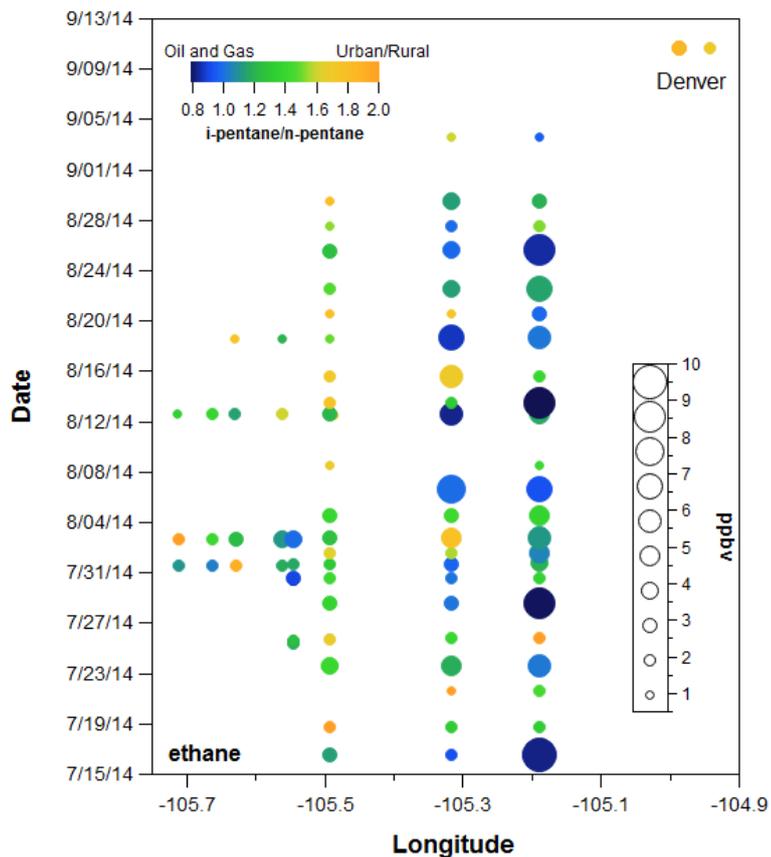
**Figure 8. VOC canister data plotted by longitude and date with ethane mixing ratio represented by the size of each point and the i-
to n-penane represented by the color. Locations correspond to transect samples shown in Figure 2.**
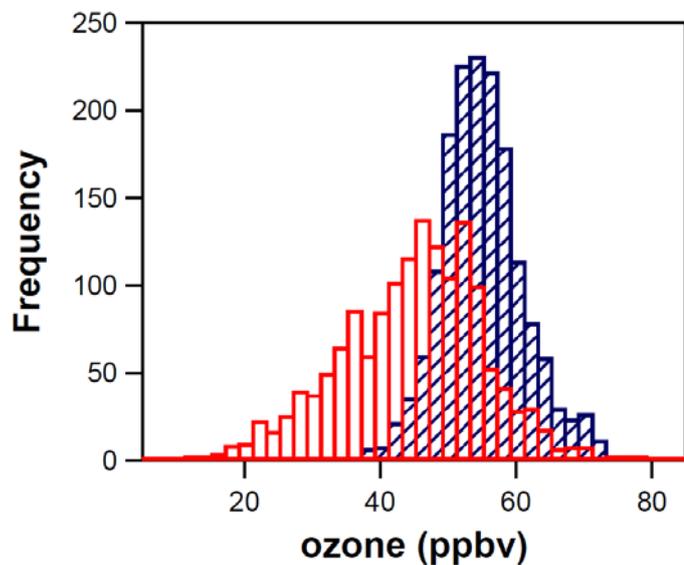
Figure 9. Distribution of the O₃ mixing ratios at the ROMO-LP (red) and ROMO-TR (blue) sites for the entire study period.
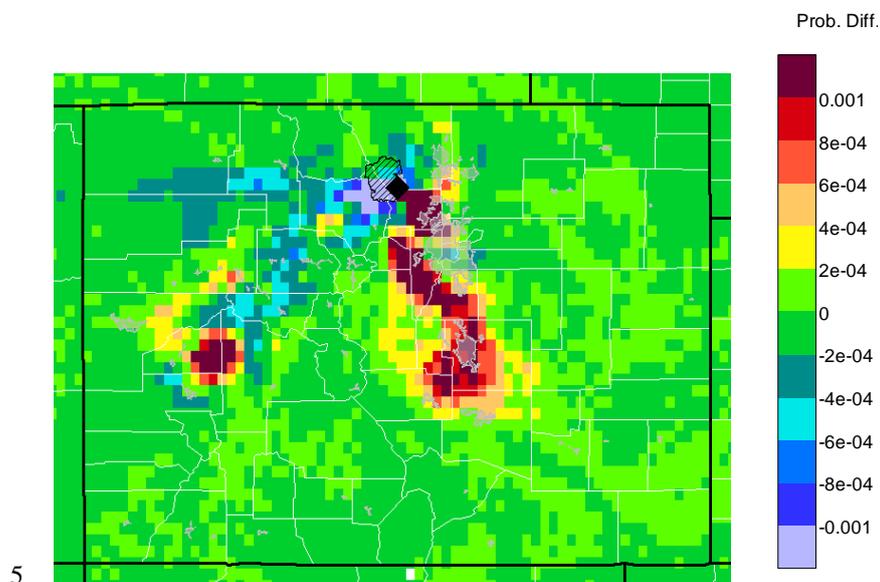
Figure 10. Differences between upwind transport during hours of 90ᵗʰ percentile or higher mixing ratios and average conditions during the study (HRT-ORT) for O₃. Warm colors indicate areas that were more likely than average to be upwind during the 2 days prior to a high mixing ratio measurement at ROMO-LP. Cool colors indicate areas that were less likely to be upwind, while areas in green had similar likelihoods of being upwind during average and high mixing ratio hours.
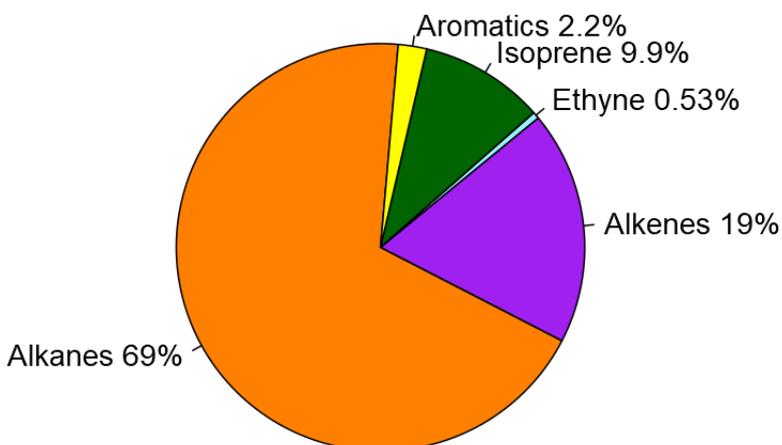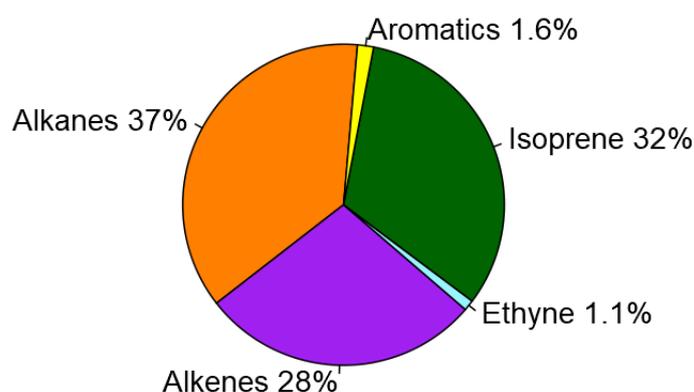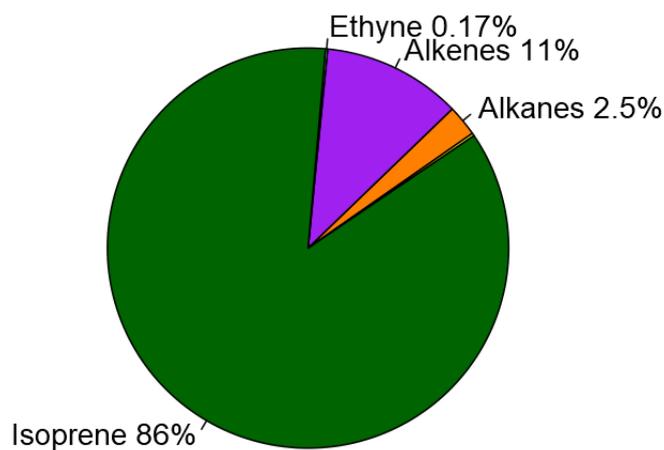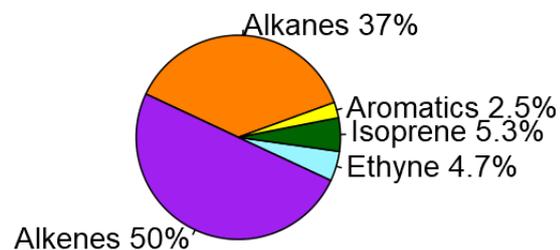
Figure 11. Contributions to •OH reactivity (OHR) for the high O₃ days for peak O₃ hours as
shown in Table 2. Days with high O₃ were grouped by the ratio of i- to n-pentane for oil and gas influenced and urban influenced

air masses. Background days, defined by the lowest 10th percentile for ethane, and the stratospheric influenced period are used for comparison to the high O_3 days resulting from anthropogenic activities. The size of each pie chart is proportional to the total OHR for the given type of air mass. Reactivity was calculated using rate constants from Atkinson and Avery (2003) and Atkinson (1986).
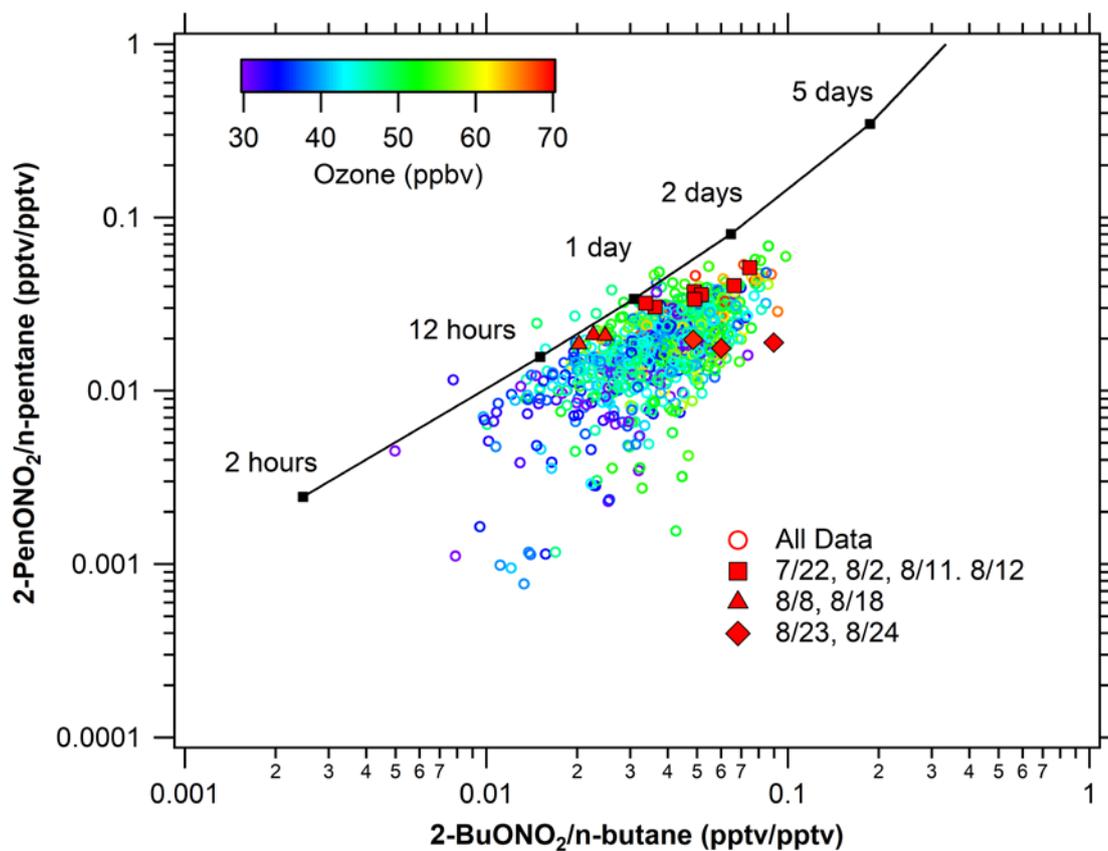
Figure 12. Photochemical age of alkyl nitrates. Comparison of observed alkyl nitrate: parent hydrocarbon ratios to predicated values provide an estimate of photochemical age.
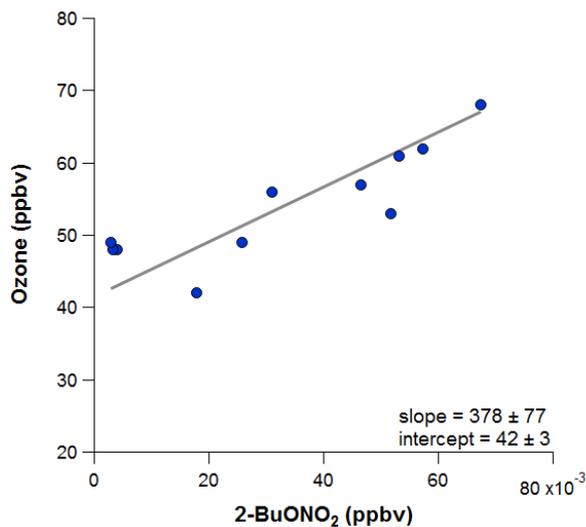
Figure 13. The orthogonal distance linear relationship of O₃ with 2-butyl nitrate during the August 18 event, when the park was clearly influenced by an air mass containing oil and gas emissions. This relationship is used in estimating the excess O₃ produced due to oil and gas emissions.
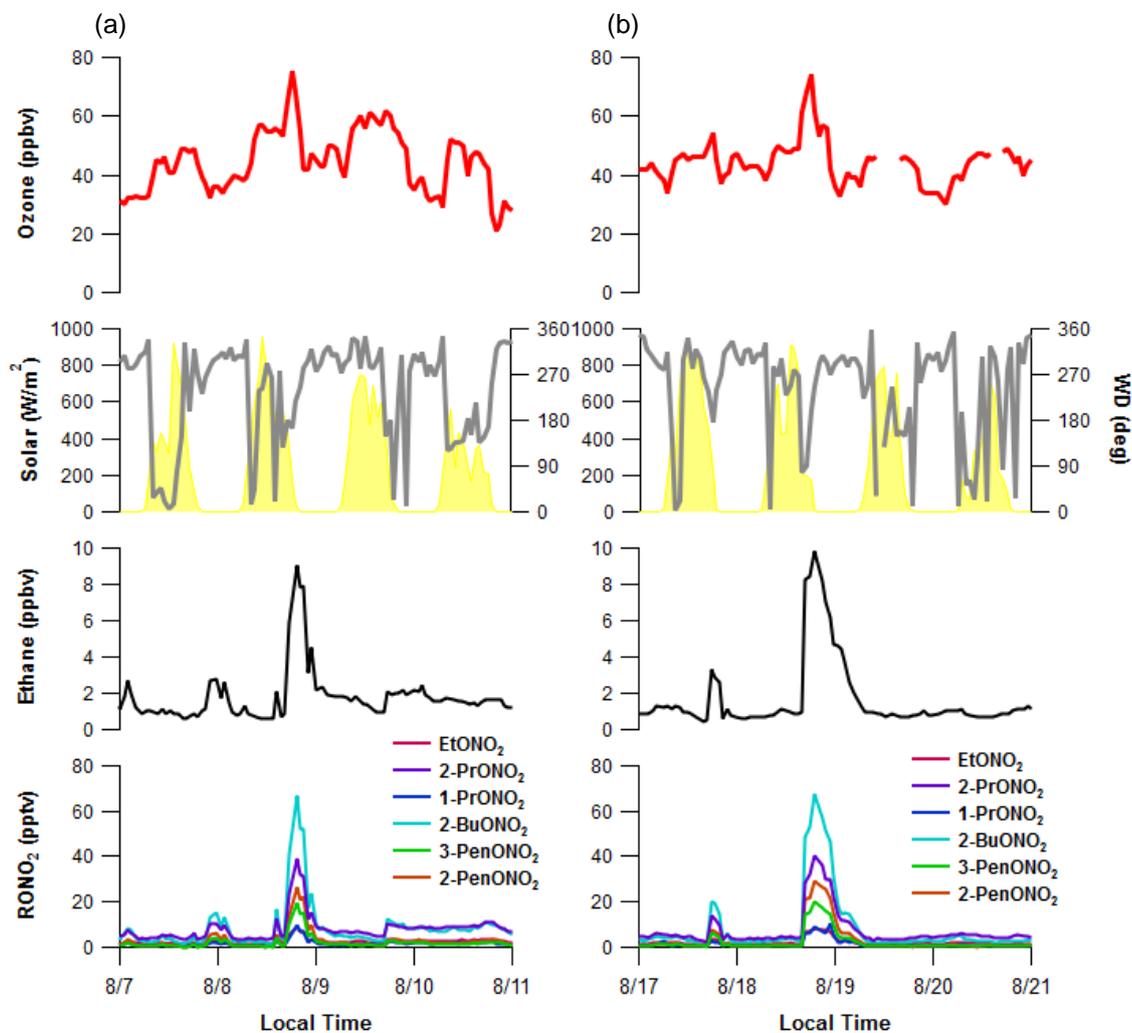
Figure 14. Time series plots of O₃, solar radiation, wind direction and the C₂-C₅ alkyl nitrates during the a) August 8 and b) August 18 upslope events.
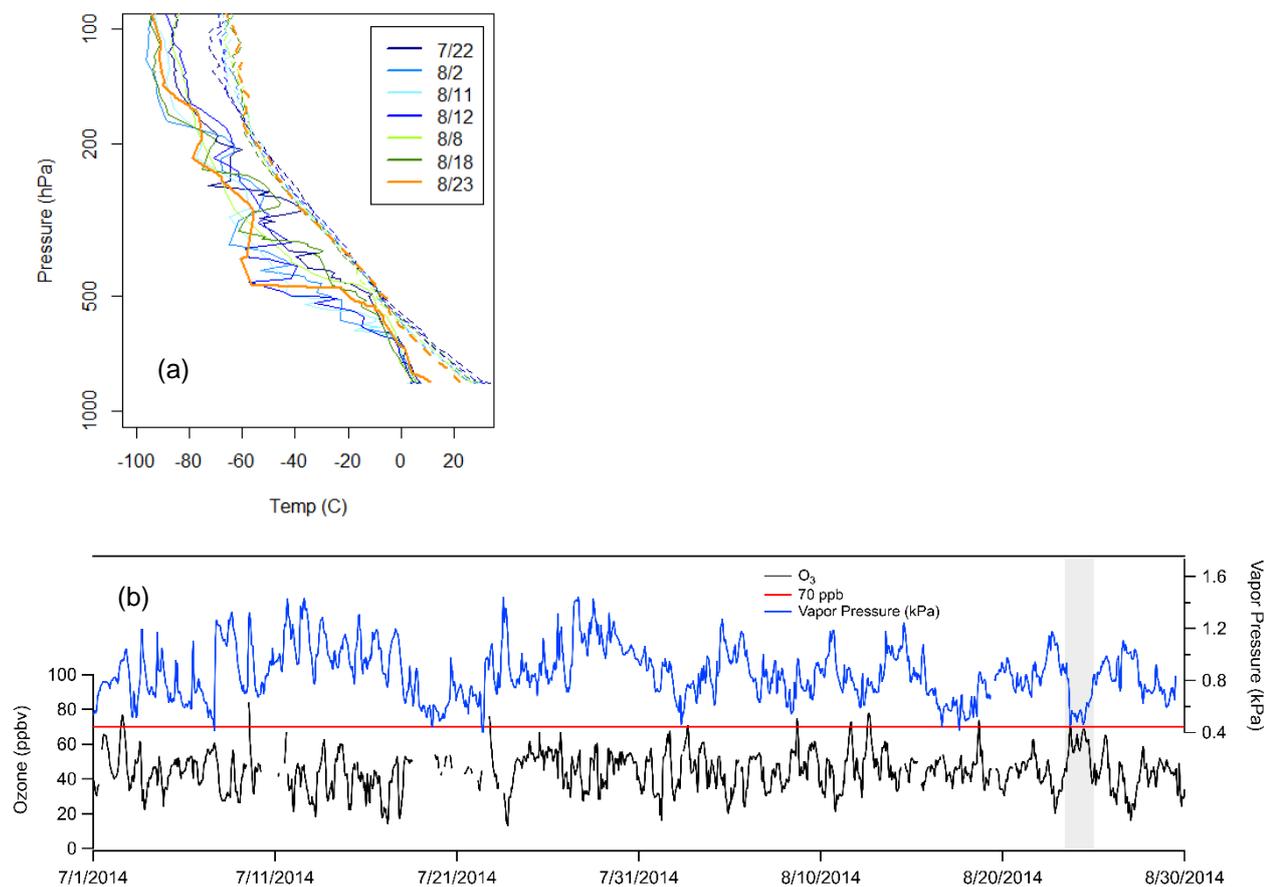
Figure 15. a) Denver soundings (http://weather.uwyo.edu/upperair/sounding.html) from high O₃ days, showing surface temperature
(dashed lines) and dewpoint (solid lines). b) Measured O₃ concentration and water vapor at ROMO-LP during the study period.
The event from August 23 is highlighted with gray shading.

Table 1. VOCs measured using the *in situ* GC system and PTR-MS at ROMO-LP. Also denoted are gases reported from the transect canister samples. Statistics are given for the GC and select PTR-MS data.

		Average	Median	Max.	Min.	Standard Deviation	Measured in Canister Samples?
		Mixing Ratio (ppt)					
ethane	GC	1516	1255	9800	485.0	1061	x
propane	GC	872.0	616	6842	65.2	991	x
i-butane	GC	103.0	61.3	1158	11.1	141.0	x
n-butane	GC	233.0	110.0	2978	18.8	374.0	x
ethyne	GC	168.7	141.4	1547	17.3	129.4	x
i-pentane	GC	144.0	61.9	2095	7.3	168.0	x
n-pentane	GC	97.5	50.7	1712	8.7	151.0	x
cyclopentane	GC	7.5	4.9	148.0	0.6	9.7	
n-hexane	GC	34.0	16.0	1113	1.8	70.6	x
n-heptane	GC	15.6	8.7	396.0	0.5	29.4	x
n-octane	GC	13.4	6.4	304.0	1.0	26.4	
n-nonane	GC	10.6	5.7	151.0	1.1	17.7	x
ethene	GC	113.0	87.0	1497	26.3	111.0	
propene	GC	712.0	72.9	762.0	3.6	53.4	
t-2-butene	GC	4.7	3.2	80.6	1.0	5.7	
1-butene	GC	6.5	5.2	84.8	1.1	6.0	
i-butene	GC	14.7	12.6	74.0	1.7	8.5	
c-2-butene	GC	5.6	3.4	76.3	1.0	7.1	
isoprene	GC	113.6	55.1	1559	1.0	185.5	x
a-pinene	GC	68.6	25.8	602.7	1.0	98.2	x
b-pinene	GC	84.4	39.7	821.3	1.0	110.4	x
toluene	GC	48.8	27.4	820.0	2.3	76.5	x
ethylbenzene	GC	17.6	7.5	128.0	1.1	26.6	x

m+p-xylene	GC	50.9	11.8	471.0	2.0	92.9	x
o-xylene	GC	20.2	5.5	168.0	1.3	32.2	x
C_2HCl_3	GC	0.7	0.5	3.0	0.1	0.6	x
C_2Cl_4	GC	2.0	1.6	10.2	0.9	1.1	x
CH_3I	GC	0.5	0.5	1.8	0.0	0.3	
CH_2Br_2	GC	0.8	0.8	1.1	0.5	0.1	
$CHBrCl_2$	GC	0.8	0.7	1.6	0.4	0.2	
$CHBr_3$	GC	0.6	0.6	1.6	0.1	0.2	
$MeONO_2$	GC	6.0	5.9	11.7	3.2	1.2	x
$EtONO_2$	GC	2.7	2.4	11.8	1.1	1.4	x
$i\text{-}PrONO_2$	GC	7.6	5.7	39.0	1.8	5.5	x
$n\text{-}PrONO_2$	GC	1.8	1.3	10.1	0.4	1.3	x
$2\text{-}BuONO_2$	GC	7.8	4.4	67.5	0.8	9.2	x
$3\text{-}PenONO_2$	GC	1.9	0.9	19.9	0.1	2.6	x
$2\text{-}PenONO_2$	GC	2.4	1.2	29.2	0.1	3.7	x
methanol	PTRMS	2780	2510	11400	660	1330	
acetaldehyde	PTRMS	380	320	2220	60	250	
acetone	PTRMS	1270	1100	3790	120	670	x
acetic acid	PTRMS	1060	1010	3800	50	540	
MVK+MACR	PTRMS	137	122	414	25	65	
MEK	PTRMS	130	100	670	20	91	
monoterpenes	PTRMS	160	130	680	50	92	
benzene	PTRMS	85	76	370	30	35	x
toluene	PTRMS	63	53	560	20	39	
C_8 aromatics	PTRMS	120	110	770	40	60	
C_9 aromatics	PTRMS	110	100	340	80	50	

Table 2. Summary of high O₃ events where at least 1 hour exceeded 70 ppb. Timing of the exceedance and the average peak concentration for both the Longs Peak and Trail Ridge monitoring sites are also included. Times shown are local.

	ROMO-LP			ROMO-TR	
	hours exceeding 70 pbb	average for exceedance	i- to n-pentane	hours exceeding 70 ppb	average for exceedance
7/22/2014	17:00-20:00	74	1.12	17:00-22:00	77
8/2/2014	17:00	71	1.05	20:00-21:00	71
8/8/2014	17:00	75	0.97	–	–
8/11/2014	15:00-16:00	73	1.44	17:00, 20:00, 21:00	70
8/12/2014	14:00-17:00	76	1.32	15:00-20:00	74
8/18/2014	17:00	74	0.97	20:00-21:00	72
8/23/2014	17:00	72	1.36	–	–
8/24/2014	–	–	–	11:00	70

Table 3. Summary of the O₃/RONO₂ slopes (ppbv/ppbv), intercept values (ppbv), the range of O₃ attributable to each parent alkane, and the average O₃ attributable to each parent alkane based on the correlation in each of the O₃-alkyl nitrate scatter plots for the upslope events on August 8 and August 18. An orthogonal distance regression was used to determine the slope and intercept.

	$RONO_2$	Slope $(O_3/RONO_2)$	Intercept (ppbv)	Attributed O_3 Range Min–Max (ppbv)	Attributed O_3 Range Ave (ppbv)
August 8 Event	$EtONO2$	2.9E+03	42	20 – 26	22
16:00-18:00	$i\text{-}PrONO2$	7.9E+02	40	24 – 30	27
(MST)	$n\text{-}PrONO2$	2.6E+03	44	17 – 24	20
	$2\text{-}BuONO2$	4.2E+02	43	22 – 28	24
	$3\text{-}PenONO2$	1.1E+03	46	16 – 21	18
	$2\text{-}PenONO2$	8.7E+02	45	18 – 23	20
August 18 Event	$EtONO2$	2.7E+03	41	18 – 23	20
15:00-18:00	$i\text{-}PrONO2$	6.3E+02	41	19 – 25	21
(MST)	$n\text{-}PrONO2$	2.1E+03	44	13 – 21	16
	$2\text{-}BuONO2$	3.8E+02	42	18 – 26	21
	$3\text{-}PenONO2$	1.0E+03	45	14 – 20	17
	$2\text{-}PenONO2$	7.3E+02	45	16 – 21	18

Table 4. Percentage contributions of the light alkanes to the alkane OHR during the oil and gas influenced events at ROMO during FRAPPÉ (Total alkane OHR =0.62 s⁻¹) and from measurements at the BAO and PAO ([1]Swarthout et al. (2013), [2]McDuffie et al. (2016), [3]Abeleria et al. (2017), [4]Halliday et al. (2016)).

	ROMO Summer 2014	BAO Winter 2011[1]	BAO Summer 2012[2]	BAO Spring 2015[3]	BAO Summer 2015[3]	PAO [5] Summer 2014[4]
ethane	8	8	6	11	10	7
propane	26	27	22	30	19	22
i-butane	9	9	9	6	7	9
n-butane	24	25	24	15	19	23
i-pentane	13	11	14	15	19	13
n-pentane	13	12	16	15	19	15
C_6-C_9	8	7	10	8	7	11
$\sum OHR_{alkane}$ (s⁻¹)	0.61	1.59	1.52	0.66	1.04	3.07